Article:
Folena, M, Barker, R, Pessu, F et al. (2020) CO2 Top-of-line-corrosion; assessing the role of acetic acid on general and pitting corrosion. Corrosion. 3569. ISSN: 0010-9312

https://doi.org/10.5006/3569

CORROSION
The Journal of Science and Engineering

CO_2 Top-of-line-corrosion; assessing the role of acetic acid on general and pitting corrosion

Journal:	*CORROSION*
Manuscript ID	CJ-2004-OA-3569.R2
Manuscript Type:	Original Article
Date Submitted by the Author:	n/a
Complete List of Authors:	FOLENA, MARIANA; Federal University of Rio de Janeiro, COPPE/LabCorr - Metallurgical and Materials Engineerings Barker, Richard; Institute of Functional Surfaces, Mechanical Engineering Pessu, Frederick; University of Leeds, School of Mechanical Engineering PONCIANO GOMES, JOSE ANTONIO; Federal University of Rio de Janeiro, Metallurgy and Materials Neville, Anne; University of Leeds, School of Mechanical Engineering
Key Words:	acetic acids, corrosion monitoring, vapor phase, multiphase, oil and gas, localized corrosion

CO_2 Top-of-line-corrosion; assessing the role of acetic acid on general and pitting corrosion

Mariana Costa Folena, ‡,*,** *Richard Barker,* ** *Frederick Pessu,* ** *José Antônio da Cunha Ponciano* * *and Anne Neville* **

‡Corresponding author. E-mail: mnmcf@leeds.ac.uk / marianafolena@metalmat.ufrj.br .

* LabCorr/UFRJ, Av. Athos da Silveira Ramos, 149 – Centro de Tecnologia UFRJ, Rio de Janeiro, RJ, 21941-972, Brazil

** Institute of Functional Surfaces (iFS), School of Mechanical Engineering, University of Leeds, Leeds, LS2 9JT, UK.

ABSTRACT

Based on a review of both literature and field data, it is apparent that the role of acetic acid (HAc) in oilfield brines is both extremely complex and somewhat controversial. Although it is commonly believed that the presence of this organic compound enhances both the general and the localized corrosion rate of carbon steel, HAc has recently been reported to also act as a weak general corrosion inhibitor in specific aqueous environments. These observations prompted a study into whether such behavior is apparent in a CO_2 top-of-line corrosion (TLC) scenario i.e. when HAc dissolves into condensed water which forms on the upper internal wall of carbon steel pipelines during wet-gas stratified flow. Four different water condensation rates/temperature TLC conditions were selected to investigate the role of HAc on both the kinetics and mechanism of carbon steel dissolution. A miniature three-electrode setup was developed to characterize the real-time TLC response through the implementation of electrochemical measurements. Surface analysis techniques (microscopy and profilometry) were also performed to complement the electrochemical results. Collective consideration of the corrosion response and condensate chemistry indicates that similar effects were observed compared to those reported in the literature for bulk aqueous environments, in that the introduction of HAc can result in either accentuation or a minimal/inhibitive effect on general corrosion depending upon the operating conditions. The minimal/inhibitive effects of HAc were apparent at a surface temperature of 20.5°C and water condensation rate of 0.5ml/m^2.s as no significant increase in corrosion was observed despite a significant reduction in condensate pH being generated due to the presence of HAc. X-ray photo-electron spectroscopy analysis of the inhibited steel specimen in the presence of HAc revealed the presence of iron acetate on the steel surface which may have been at least partially responsible for the observed inhibitive effect. Extended duration experiments over 96h revealed that both general and localized corrosion are not significantly affected by HAc addition at low temperature whilst the level of degradation increases at higher surface temperature over longer periods.

KEY WORDS: *acetic acid, CO_2, sweet corrosion, top-of-line corrosion*

1 INTRODUCTION

Top-of-line corrosion (TLC) is a specific corrosion mechanism observed in the oil and gas industry. This phenomena occurs under stratified or wet-gas flow regimes when the upper internal pipeline walls are sufficiently cooled (by heat transfer to the surrounding outer environment), promoting local condensation of water vapor. As fresh water condenses onto the steel surface carbon dioxide (CO_2) and organic acids dissolving into the condensed water generate a change in the solution chemistry reducing condensate pH. Such changes ultimately influences the corrosion kinetics of the contacting carbon steel. Depending on the temperature and water condensation rate (WCR) two scenarios might take place during the water condensate renewal cycle. First, the steel dissolution might result in Fe^{2+} saturation and pH increase leading to the formation of a protective $FeCO_3$ film. Second, no protective film is formed and corrosion continuously take place on the bare steel surface.

In the oil and gas industry, the majority of hydrocarbon reservoirs produce both acid gases and volatile organic acids in conjunction with formation brine and hydrocarbons. These gases and volatile compounds create highly corrosive condensate chemistries for carbon steel pipelines. Organic acids such as acetic acid (HAc) are well known to accentuate TLC of carbon steel dramatically across a range of conditions, with this particular acid's role receiving significant research attention. However, the underlying mechanism has not been explored extensively until fairly recently.[1] The influence of HAc on CO_2 corrosion needs to be studied holistically, as it can have a multitude of synergistic or antagonistic roles, including increasing the cathodic reaction rate (via lowering solution pH and through the ability of HAc to facilitate a 'buffering' effect at the steel surface), inhibiting the anodic and cathodic charge-transfer reactions (through inhibition of the cathodic hydrogen ion reduction reaction and the anodic iron dissolution reaction), and changing the solubility and protective characteristics of corrosion products.[2,3,4,5,6]

Interestingly, some studies have shown that in particular bulk fluid chemistries (pH range within 3-5) in dynamic conditions, the addition of HAc can be minimal in terms of influencing the corrosion rate of carbon steel, even resulting in a diminution in general corrosion rate under a given controlled solution pH. Such observations have been attributed to the suppression of the anodic dissolution reaction and cathodic charge-transfer reaction due to the ability of HAc to chemically adsorb onto the metal surface.[4,7,8,9] Although the role of HAc has recently received increased attention with respect to bulk aqueous environments, the same effect has not been characterized for a TLC environment (i.e. a process under condensation corrosion). This study investigates whether, under certain conditions, HAc can also have a negligible or inhibitive effect on corrosion of carbon steel in specific TLC environments, despite being dosed at comparable field concentrations.

Based on previous studies on the role of HAc in CO_2 TLC conditions, a set of laboratory-scale experiments and conditions are devised here, consisting of four different water condensation rates and temperature combinations commonly reported or evaluated in TLC cases. For this purpose, a real-time corrosion monitoring setup[10] was implemented in order to evaluate the transient corrosion response throughout experiments, and evaluate the role of HAc across a range of environments.

2 EXPERIMENTAL PROCEDURES

In the present study, mass loss and electrochemical test specimens (shown in Figure 1) were used in order to obtain corrosion rate data. The mass loss specimens consisted of cylindrical coupons 10mm in diameter and 6mm thick, with an exposed area to the vapor phase of 0.785cm^2. Both mass loss and electrochemical specimens were manufactured from the same API 5L X65 carbon steel stock bar, which possessed a ferritic-pearlitic microstructure and has the chemical composition shown in Table 1.

The miniature three-electrode setup used to monitor the changes in corrosion rate throughout the course of the experiment consisted of three metallic electrodes mounted inside a carbon steel sample with the same outer geometry as the mass loss specimens (to ensure comparable heat-transfer to both specimen configurations). The working electrode consists of a 1mm diameter X65 steel pin. The reference and counter electrodes both comprised of a 1mm diameter Hastelloy® c-276 wire as shown in Figure 1. Each electrode is individually isolated by a lacquer coating and shrink wrap tubing. The miniature solid electrode set up has been used in a previous study by de Carvalho *et al.*[10] and in both studies produced comparable results to the conventional three-electrode setup in solution chemistries indicative of the condensate produced in these TLC experiments.

The exposed surfaces of the test specimens were wet-ground up to 1200 silicon carbide (SiC) grit paper to produce a planar, clean surface. A thermocouple probe was placed laterally across the 10mm diameter specimens in specific experiments, touching its exposed surface for

surface temperature (T_s) measurements; these specimens were not used for mass loss measurement due to the potential occurrence of galvanic effects. A bespoke laboratory scale TLC rig was used in this study,[10] with the schematic drawing provided in Figure 2. The setup consists of a 2L glass cell with a specific custom lid integrated with an internal channeled matrix and test specimen slots, allowing flow of refrigerant to cool the surface of the TLC specimens to specific temperatures. The test specimen slot on the channeled lid allows the simulation of 12 o'clock position of a horizontal 6 inch (152.4mm) diameter pipeline.

The selected gas temperature (T_g) and surface temperature (T_s) were achieved by controlling the bulk fluid temperature in the 2L glass beaker using a hot plate. The refrigerant temperature (T_{ext}) in the channeled matrix was controlled using a chiller system. The same test methodology, used to reach the aforementioned desired conditions, and accuracy of temperature control for this specific rig can be found in previous work.[10]

The bulk test solution consisted of CO_2-saturated 3.5 wt.% NaCl solution with the presence and absence of 1000 ppm HAc, which was purged with CO_2 for a minimum of 12h prior to each experiment, to minimize the dissolved oxygen content. CO_2 was continuously bubbled into the cell throughout the test to avoid oxygen ingress.

Dissolved oxygen measurements were performed after each test using CHEMets colorimetric test kits using the Rhodazine D method. When in contact with tested sample the Rhodazine D compound in reduced form reacts with dissolved oxygen to form a bright pink reaction product. All the TLC tests showed that the saturation of the system was valid and produced dissolved oxygen readings of less than 50 ppb.

The volume of condensed water in the graded collector was recorded and the water condensation rate (*WCR*) was calculated using Equation (1):

$$WCR = V_w/(L_s.t_c) \qquad (1)$$

where *WCR* is the water condensation rate in mL/m^{2}s, V_w is the volume of condensed water in mL, t_c is the duration over which the condensed liquid is collected in s, and L_s is the internal area of the lid surface exposed to the vapor condensation (m^2).[10]

The condensate collector itself was also deaerated by bubbling continuously with CO_2 during the experiment to maintain the same environmental conditions. The pH of bulk solution was measured at the beginning and at the end of each test using an automatic temperature correction pH probe. Additionally, condensate samples from all four different WCRs were collected to perform ionic chromatography analysis in order to quantify the amount of HAc that evaporated from the bulk solution and reached the top-of-line section. The ionic chromatography was performed with a ThermoScientific ICS-5000 system. Cations were separated with AS19 analytical column (2mm × 250mm). The system was employed with a guard column AG 19 (2mm × 50mm). All sample runs were performed using both the guard and the analytical column.

Electrochemical measurements were performed using the miniature electrodes using a computer controlled ACM Gill 8 potentiostat. Three electrochemical techniques were implemented in total. Linear polarization resistance (LPR) and electrochemical impedance spectroscopy (EIS) were employed to determine the *in situ* corrosion rate of the X65 carbon steel specimens. LPR measurements were performed by polarizing the sample ±15 mV vs the open circuit potential (OCP) at a scan rate of 0.25 mV/s to obtain a polarization resistance (R_p) and were undertaken every 20 minutes. The solution resistance (R_s) was measured over the course of the experiment using EIS. These measurement were performed

using an amplitude of ±15 mV vs the OCP and a frequency range from 20 kHz to 0.1 Hz. These parameters were chosen taking into account previous work[10] which have shown that the system is stable enough to perform such analysis during the acquisition period.

The value of R_p was corrected for R_s ($\Omega.cm^2$) and ultimately used to determine the corrosion rate with time using the Stern-Geary relationship in conjunction with Faraday's Law. For tests performed in the 4 different WCRs the average of R_s values were 5.6 ± 0.9 $\Omega.cm^2$ in solutions without HAc and 4.3 ± 0.6 $\Omega.cm^2$ in the presence of HAc.

Due to the droplet cycle process, there were some instances in which the electrochemical measurements were interrupted, resulting in noisy or erratic LPR responses. This phenomena is associated with the intermittency of droplet contact between all three of the electrode probes. Under such instances, two scenarios can be hypothesized to explain the anomalous electrochemical responses:

1) The droplet/liquid film is no longer in contact with the carbon steel electrode, and corrosion ceases prior to the formation and/or growth of a droplet.

2) A droplet/liquid film does exist at the carbon steel electrode surface, resulting in continued corrosion of the steel sample. However, electrochemical measurements are prohibited due to a lack of a consistent contact between the electrolyte and all three electrodes.

Each of the two aforementioned scenarios results in a different interpretation of the magnitude of corrosion rate during these intermittent periods, and it is likely that both scenarios occur during the experiment. However, the proportion to which each occurs in not clear. In order to produce conservative predictions of corrosion rates from the miniature electrodes in instances where electrochemical measurements were not possible, the corrosion rate was determined via interpolation between the nearest measurements in time either side of any erratic reading. (This is as opposed to assuming a corrosion rate of zero at such points.) To highlight the significance of processing such measurements in this manner, it was determined that setting such values at 0 mm/year resulted in a reduction of the corrosion rate by approximately ~10-15% in the most extreme cases compared to the interpolation method. This result is smaller than the error associated with repeat measurements of the experiment.

After completion of each 20 h experiment, Tafel polarization curves were collected by performing individual anodic and cathodic sweeps (on separate test specimens), starting from OCP and scanning to -150mV vs. OCP, for the cathodic branch, and to +150mV vs. OCP, for the anodic branch, at a scan rate of 0.5mV/s. From the polarization curves produced, it was possible to determine the anodic (β_a) and cathodic (β_c) Tafel constants in mV/decade by measuring their respective gradient over regions where linearity was observed (on an E vs log(i) plot). Then determine the Stern-Geary coefficient (B), for each experiment, and ultimately the corrosion current density (i_{corr}) (Equation (2)):

$$i_{corr} = \frac{B}{R_{ct}} = \frac{1}{R_{ct} 2.303} \frac{\beta_a \beta_c}{(\beta_a + \beta_c)} \quad (2)$$

where B is the Stern-Geary coefficient, β_a is the magnitude of the anodic Tafel constant, and β_c is the magnitude of the cathodic Tafel constant (determined in separate experiments). The value of i_{corr} was then used in conjunction with Faraday's Law and an appropriate conversion factor to obtain the corrosion rate in mm/year, as shown in the Equation (3), which was converted into a rate of thickness loss in mm/year, in accordance to ASTM G102.[11]

$$CR = K\frac{i_{corr}M_{Fe}}{nF\rho} \quad (3)$$

where *K* is a conversion factor to obtain corrosion rate (*CR*) in units of mm/year (K = 3.16x10^8), M_{Fe} is the molar mass of iron (55.8g), *n* is the number of electrons freed in the corrosion reaction (2 electrons – Fe^{2+}) and ρ is the density of steel (7.87g/cm^3).

From analysis of the corrosion rate (CR) vs time curves produced from the electrochemical measurements, an average corrosion rate (ACR) was determined over the duration of each 20h experiment, making it possible to compare the results obtained with the mass loss experiments performed in this study, as well as the work of other researchers.

Four different experimental conditions were generated by setting various combinations of T_g and T_{ext} in accordance with values reported in the literature.[12,13] The experimental matrix of tests performed in this study are presented in Table 2. In summary, experiments were performed at two WCR values below the 0.25ml/m^2.s 'threshold' and two above this value, with the latter two values simulating more severe conditions analogous to a system whereby external insulation may have failed in the field. Each of the four experimental conditions were studied in both the absence and presence of 1000ppm HAc.

In order to accurately evaluate and quantify the extent of localized TLC, long term tests (96h) were also performed. Based on the corrosion responses from the 20h experiments, the highest and lowest surface temperature were chosen as the conditions for longer duration tests, since these represented the most and least aggressive conditions for general TLC, respectively.

In order to understand the role of HAc in TLC, different surface analysis methods were implemented to complement the corrosion rate data extracted from mass loss and electrochemical measurement. Scanning electron microscopy (SEM) analysis was performed using a HITACHI Tabletop Microscope TM3030 for observation of the corrosion features. In addition, a Bruker NPFlex 3D interferometer was used to analyze the roughness of the corroded surface of the mass loss specimens using a 20x magnification lens. Three mass loss specimens were analyzed for each test condition using profilometry for roughness and pitting/localized corrosion. A surface area of 2mm × 2mm was analyzed on each of the three mass loss specimens. According to ASTM G46-94[12] standard, an average of the 10 deepest pits and the maximum pit depth (based on relative pit depth measurement after removal of corrosion products) should be used for pit damage characterization.

Fourier transform infrared spectroscopy (FTIR) analysis was performed with a PerkinElmer Spectrum 100 with Universal ATR accessory fitted, and recorded between 600 and 4000 cm^{-1}. This technique was used to obtain chemical information about the organic corrosion product film adsorbed on the surface of the sample. Complementary, X-ray photoelectron spectroscopy (XPS) characterization was conducted using a Thermo NEXSA with an X-ray source of Al Kα and analysis spot size of 100µm, to corroborate the investigation of iron acetate layer on the steel surface.

3 RESULTS AND DISCUSSION

3.1 Corrosion Rate Response in CO_2 Top-of-line Corrosion Environments over 20 h

Top-of-line corrosion rates from electrochemical measurements every 20 minutes over 20h across four different test environments both with and without 1000ppm HAc are provided in Figure 3. Each graph from Figure 3(a) to (d) presents the real-time measurements of two tests at each condition. In addition, Figure 3(e) provides an indication as to the frequency of measurements using the miniature electrode configuration, where there appeared to be a discontinuous electrochemical circuit. It shows what percentage of the measurements could not be used to deduce the corrosion rate. The implications of such intermittency are analyzed and discussed in due course for each experimental condition.

The average corrosion rates over 20h in all the TLC environments without HAc ranged between 0.5 mm/year and 1.5 mm/year, agreeing with the range of values reported in previous studies under comparable conditions.[10,13,14,15] The corrosion rate values increased with both increase in surface temperature and water condensation rate as expected and stated by previous researchers in conditions without film formation.[10] Although some test environments suggested a possible increase in corrosion rate with time over the course of the 20 h experiment (e.g. at the WCR of 0.81ml/m^2.s in Figure 3(a)), this increase could arguably lie within experimental error. However, such an observed increase with time can be explained either by increased surface roughening (and hence an increase in the true contact area between the test specimen and electrolyte) due to corrosion, and/or preferential dissolution of ferrite leaving behind an iron carbide (Fe_3C) phase, which is known to lead to an enhancement in the kinetics of hydrogen evolution, and hence increase the rate of iron dissolution.[3,14]

The addition of 1000ppm HAc into the bulk brine solution resulted in a significant increase in the TLC rate for three of the four environments. For the specimens tested at T_s = 50.3^{o}C/WCR = 0.5ml/m^2.s and T_s = 42.5^{o}C/WCR = 0.81ml/m^2.s, the average corrosion rate increased with time from 0.8 mm/year to 2.8 mm/year, and from 1.4 mm/year to 3.0 mm/year, respectively (Figures 4(a) and (b)).

At a surface temperature of 32.5^{o}C and WCR of 0.07 ml/m^2.s, regarding the corrosion rate vs time plot (Figure 3(d)), the initial corrosion rate was ~2.5 mm/year at the beginning of the tests in the presence of 1000ppm HAc, rapidly increasing to 4.4 mm/year after 120 minutes of immersion, and then decreasing during the remainder of the test.

For the lowest surface temperature evaluated (20.5^{o}C) with a WCR of 0.2ml/m^2.s, shown in Figure 3(c)), the presence of 1000ppm HAc did not significantly accentuate of the corrosion kinetics for X65 steel, which remained ~0.5 mm/year throughout the 20 h experiment. Through consideration of the corrosion response, there is a suggestion that the addition of 1000ppm HAc produces a reduction in corrosion rate, although this could be argued as insignificant considering the experimental error. Nonetheless, it is clear that the addition of 1000ppm HAc produces no significant increase in corrosion rate, even though HAc facilitates a reduction in condensate pH (as discussed and indicated later). Such observations suggest HAc is acting as a weak corrosion inhibitor, a feature which has been reported in low test temperature environments where the synergism between HAc and temperature is less significant and the chemical adsorption of HAc or the associated iron acetate layer and/or iron acetate complex on the steel surface is substantial and dominant enough to suppress both the anodic and cathodic charge-transfer reactions.[8,9]

Referring to Figure 3(e) the percentage of discontinuous electrochemical measurements increased with the presence of HAc from 12.5% to 20%. The tests conducted at lower temperatures (20.5^{o}C and 32.5^{o}C) and hence, lower WCRs, resulted in only 10% and around 15% of 'non-connectivity' data for 0ppm and 1000ppm HAc, respectively. The frequency of such erratic measurements can be at least partially related to the condensation and droplet formation rates, which are responsible for maintaining collective wetting of the miniature electrode surfaces. However, given the substantial influence of HAc on the percentage of valuable extracted data from the experiments, it appears that the WCR may not be the only controlling factor.

We suggest that there might be an apparent synergistic effect between WCR, the HAc and surface temperature, since at high T_s and HAc presence there was an increase in 'non- connectivity' measurements. Furthermore, Okafor and Nesic (2007)[16] observed that the presence of HAc on TLC has the ability to change the condensation mode from filmwise to dropwise condensation, which could also lead to increased intermittency of data measurements.

The average corrosion rate from the real time corrosion tests was calculated and compared to those acquired through mass loss tests in order to determine the accuracy and validity of the electrochemical technique. As shown in Figure 4(a), a high level of agreement exists between these two methodologies. Additionally, a comparative graph was plotted (Figure 4(b)), which shows that the electrochemical responses acquired with the developed miniature electrode configuration is in accordance with values from the literature under similar conditions.

Furthermore, one of the main parameters that influences TLC rate (and has received little research attention until recently) is T_s. Since corrosion is an interface phenomenon, the temperature at the steel-electrolyte interface will undoubtedly influence the steel response to the corrosive environment, as highlighted in recent studies by Islam et al.[17] and by De Carvalho et al.[10]. The influence of T_s on the corrosion rate response is plotted in Figure 4(b) for experiments in the absence of HAc. Figure 4(b) shows that in the absence of HAc, a good agreement is observed between corrosion rate and T_s in environments where no corrosion products form. This strong agreement is observed despite difference in WCR between each author for the given values of T_s, demonstrating that T_s has the dominant effect across the collective environments considered in these studies.

Considering Figure 4(a) and (b), there is a progressive increase in corrosion rate with T_s in the absence of HAc, following the familiar Arrhenius trend in the absence of formation of any protective corrosion products (the absence of which is supported by SEM observations presented later). In the presence of 1000ppm HAc, the observed trend is not as straightforward, with the corrosion rate appearing to converge to a maximum rate as T_s is increased. This indicates a much more complex process occurring within the condensate and/or at the steel surface. The accentuated dissolution rate of the steel beyond 20°C will have a more profound effect on the evolution of solution chemistry in the droplet, coupled with the potential inhibition effect and the known synergy between HAc and temperature, generates an environment whereby the prediction of corrosion kinetics is particularly challenging.[4,5]

Table 3 summarizes the average corrosion rate in each test environment, based on the electrochemical data acquired over 20h. The greatest increase in corrosion rate due to the addition of HAc (303%) occurred at the lowest WCR (0.07 ml/m^2.s) and temperature of 32.5°C, whilst in the test performed at T_s = 20.5°C and WCR = 0.2 ml/m^2.s, there was an average decrease in the corrosion rate of ~19% when HAc was added, although this is not significant when considering the experimental error associated with repetitions. As stated previously, such a decrease, or lack of accentuation in corrosion rate in a more aggressive condensate chemistry is likely attributable to the adsorption of HAc or an associated complex/iron acetate acting as a weak corrosion inhibitor.[8,9]

In the remaining other three test environments, the accentuation of corrosion rate can be attributed to the ability of HAc to enhance the rate of the cathodic reaction, increasing the overall corrosion kinetics. Under these conditions, the beneficial inhibitory effects of HAc are outweighed by its ability to accelerate the cathodic hydrogen reduction reaction by lowering condensate pH (providing a greater source of H^+), as well as providing a 'buffering effect' to enhance the cathodic reaction even further.

Referring to the literature, bulk fluid electrochemical corrosion experiments performed with carbon steel in the presence of HAc showed that anodic and cathodic current densities close to OCP in Tafel plots at near room temperature were progressively suppressed with increasing HAc

concentration, suggesting HAc does indeed slightly inhibit both charge-transfer reactions.[5,9] Gulbrandsen and Bilkova[8] also established that HAc or Ac^- may inhibit electrochemical reactions, in particular the anodic reaction at room temperature, suppressing general corrosion. They performed rotating cylinder electrode experiments with X65 steel in 0.3 wt.% NaCl brine saturated with CO_2 both with and without HAc. The tests showed that by introducing 200ppm of HAc into the system, the final corrosion rate would drop from 4 mm/year (with no HAc) to 1.5 - 2 mm/year, whilst the open circuit potential (OCP) would increase from -0.67V to -0.60V. However, the addition of the acid changed the morphology of corrosion attack from uniform to localized, showing deep pits on the exposed surface.

Figure 5 presents repetitions of Tafel polarization curves for carbon steel exposed to each of the four environments after 20h of TLC exposure, with the y-axis representing the applied potential vs the OCP at the end of each individual test. This has been presented in such a manner due to the variability of the Hastelloy® reference electrode potential in each experimental condition and to enable easier comparison regarding the suppression or accentuation of the anodic and cathodic reactions.

By analyzing the Tafel polarization plots it can be seen that at higher T_g and T_s (Figures 5(a) and (b)) the addition of HAc clearly increases the anodic and cathodic reaction kinetics. At lower temperatures (Figure 5(d)), the level of accentuation is less pronounced, whilst at the lowest temperature (Figure 5(c)), the addition of HAc suppresses both the anodic and cathodic reactions. This suppression of reactions observed in Figure 5(c) could be attributed to inhibitive effect from HAc, which promotes a blockage of active sites for electron transfer reactions, as previously stated. These observations are in reasonable agreement with the electrochemical corrosion rate measurements at the end of each 20h experiment in Figure 3.

3.2 Miniature Electrode Non-connectivity Behavior over 20 h

As previously discussed, during TLC electrochemical measurements, periods of non-connectivity and/or anomalous data were recorded. The implications of this are shown in Figure 6, which provides a comparison between two interpretations of the real time data collected by the electrochemical measurement. For each test condition, the average corrosion rates are plotted assuming one of the two scenarios regarding the periods of non-connectivity:

1) Interpolation between points; in this scenario, the corrosion rate for the erratic readings/non-connectivity measurements were determined via interpolation between the nearest measurements in time either side of the response

2) Non-connectivity set to zero; under this scenario, any erratic reading was set to zero under the assumption that no corrosion was occurring at this instance in time.

As stated before, it is likely that a combination of both scenarios is occurring, but these two permutations represent the extremes of the process and help understand the significance of the non-connectivity measurements on the accuracy of the collected data. Consideration of the data in Figure 6 indicates that setting the non-connectivity values to zero has little bearing on the average corrosion rate, such that many responses lie within the error of the overall test repeatability.

3.3 Condensate Chemical Analysis

Table 4 shows pH measurements of the bulk solution after 20h for all four test conditions in this study. In the absence of HAc, the pH of the bulk solution varied from 3.8 to 4.2. For the environments with 1000ppm HAc added to the bulk solution, the pH values varied between 3.0 and 3.1. It is expected that the pH value in the water condensate present similar behavior as in the bulk solution, where the presence of HAc in condensate will result in a decrease of the pH in comparison to the tests conducted without the presence of the acid. To understand the extend to which HAc is able to reach the condensate, ion chromatography analysis was performed on condensate samples after each test. The methodology implemented with this technique uses a high pH buffer solution, converting all the HAc into acetate, hence, enabling measurement of the total HAc. Figure 7 shows a bar chart with the average of three replicates at each condition. The concentration of undissociated/free HAc remained similar and largely within experimental error of one another for all tested conditions, showing independence from the gas and surface temperatures, ranging from only 319 to 384ppm across all four experiments. This higher concentration of HAc in the bulk solution relative to that the measured in the condensate was expected due to the fact that HAc dissociates in the bulk solution, leaving only a proportion of HAc available to partition into the condensate. Similar values were recorded by Hinkson *et al.,* (2008)[4] when studying the chemistry of the condensate in top-of-the-line systems with the addition of 1200ppm of HAc.

Since the concentration of HAc found in the condensate across all four different surface temperatures is similar, it can be concluded the low corrosion rates observed at T_s near room temperature is not attributable to a lower HAc concentration in the condensate. This result therefore supports the theory that inhibition aided by HAc is the underlying reason behind the suppression or lack of accentuation of corrosion in the experiment at 20.5°C. Clearly, specific pH measurements of the condensate would assist in validating this theory further. However, considering that the condensate collected is a combination of that from the internal portion of the acetal TLC lid, as well as the steel surface, direct measurement of pH from the collected condensate, and/or inferring pH from the Fe^{2+}/HAc content in the condensate is likely to provide an inaccurate interpretation of the true chemistry in the droplets formed at the steel surface. Measurement of such local chemistry is the subject of future work.

3.4 Characterization of the Corroded Surface after 20 h

SEM images from the mass loss specimens after 20h with and without 1000ppm HAc (before cleaning the steel surfaces) are presented in Figure 8. The surface morphology of the steel in the absence of HAc mainly consists of undissolved Fe_3C remaining from the X65 steel microstructure due to the preferential corrosion of the ferrite phase. However, at lower surface temperature (20.5°C) it is possible to observe that the corrosion environment is less aggressive (grinding marks from preparation are still visible), agreeing with the measured electrochemical response under this condition. In the presence of 1000ppm HAc, the SEM images indicate a more aggressive corrosion environment, with the exception of the test at T_s = 20.5°C, where the inhibiting effect of HAc from corrosion measurements was most pronounced.

From all the images shown in Figure 8, no formation of crystalline corrosion product occurred on the steel surface in any condition, but rather a non-protective layer of Fe_3C is revealed after ferrite dissolution, demonstrating that all the observations reported in this work relate to non-corrosion product forming environments. Various studies on carbon steel behavior in CO_2 environments have shown that Fe_3C present in the carbon steel is revealed after the ferrite is dissolved and accumulates on the steel surface as a non-protective, porous layer.[18,19] Previous studies have hypothesized that in environments containing organic acids, a layer of iron acetate may form on the metal surface, generating a weak inhibitive effect against metal corrosion at near room temperatures[5,8,9]. However, no further investigation has been conducted to prove that the

iron acetate film is the main reason for the weak inhibitive effect observed in near room temperature conditions. In this work it is important to identify whether or not ferrous acetate forms on the surface, leading to the inhibitive effect observed in the TLC tests performed at T_s = 20.5°C. FTIR and XPS analysis were performed on the specimens tested at T_s = 20.5°C with 1000ppm HAc. The results in Figure 9 show the presence of adsorbed organic species on the steel surface after 20h of test in 1000ppm HAc which was in accordance with ferrous acetate IR (infrared) spectra. Additionally, the sample tested at 0ppm HAc shows a mainly flat spectra with no evidence of iron acetate bonds, as expected.

For acetate ions the main peaks expected are related to the stretching vibrations of the two C-O bonds of the ester group and C-H bonds of the alkyl group.[21] C-H stretching bands were found at ~2981 – 2857 and ~1464 – 1380cm^{-1} and C-O stretching bands at 1764 and 1541, which are common wavenumber values found for alkyl and ester group species found in literature, respectively.[21,22] Also, the carbonyl stretch C=O of the aliphatic ester was observed in the spectrum at 1764 and 1541cm^{-1}. Referring to Figure 9 there is a strong agreement for the main peaks of both the acquired FTIR spectra from the tested sample surface and the standard ferrous acetate data. Table 5 lists whole frequency assignments found in literature for the free acetate ion,[23] an as prepared ferrous acetate and ferrous acetate (99%, reference) studied by Kim[23] and the acquired ferrous acetate corrosion product in the present study. The weak inhibiting effect observed at low surface temperatures during the TLC tests could therefore well be credited to the formation of a thin layer of ferrous acetate at the low temperature condition.

XPS surface characterization was performed to also aid in identification of a thin film ferrous acetate layer. Figure 10 presents the C1s, O1s, and Fe2p regions of the XPS spectra scan from the mass loss specimen after 20h of TLC at T_s = 20.5°C. Fitting and quantifications analysis were performed based on literature results and implemented through CASA XPS software. For the C1s peak in Figure 10(a) the results suggest that with 1000ppm HAc, there is a peak assigned to R-O-(C=O)-R (289.09 eV) which is also identified in the standard ferrous acetate spectra and is not present in the sample with 0ppm HAc.[23,24,25] As expected, the steel samples tested with 0ppm HAc led to a spectra for C1s photoelectrons, corresponding to adventitious carbon contamination showing binding energies of common chemical states at 284.66eV (C-C, C-H), 285.51eV (C-O), and 288.33eV (C=O).[25,27,28] Still, the deconvolution of spectra also showed a small peak at 283.20eV which can be assigned to a Fe_3C thin layer, which was also observed from SEM analysis.[29,30,31]

O1s analysis also confirms the ferrous acetate presence. Figure 10(b) shows comparable curves between the ferrous acetate standard and the samples tested with 1000ppm HAc. For the samples tested with 0ppm HAc, the O1s analysis only showed the typical hydroxyl bond, which is widely observed in conjunction with Fe_2O_3.[28,29,30] These oxide and hydroxide bonds are mainly contaminants due to the sample exposure to air before storage and/or before XPS analysis.

Figure 10(c) presents the Fe2p spectra for the three different tested samples. For the sample tested without HAc, the main peaks at 711.0eV and 724.5eV can be assigned for Fe_2O_3 oxide.[31,32,33] At lower binding energy ~707 eV for both samples tested in TLC environments binding energies can be allocated to iron carbide (Fe_3C) as expected due to the corrosion process. Fe2p analysis cannot conclusively show that ferrous acetate is present, however, by combining both XPS analysis with FTIR, there is a strong suggestion that a ferrous acetate film is indeed present on the steel surface and working as a weak inhibitor to counter TLC at near room temperature.

3.5 Characterization of Pitting Top-of-line Corrosion over 20 and 96h

As discussed previously, the evaluation of pitting/localized corrosion damage in this study is divided into short term (20h – for all four test environments with and without 1000ppm HAc) and long term (96h for two selected test environments with and without 1000ppm HAc). Each of these time periods are discussed in turn.

3.5.1 Short term localized corrosion (20 h).

An example profilometry image and extracted 2D profile for a given test condition is provided in Figure 11 (WCR = 0.5mL/m^2.s and T_s = 50.25^{o}C with 0ppm HAc). Multiple scans such as these were analyzed for each test specimen exposed to TLC conditions over a duration of 20h. In total, the analysis for the 20h experiments encompassed 8 different test conditions comprising 4 different WCR/T_s combinations, both with and without 1000ppm HAc added to the bulk brine solution. The profilometry image in Figure 11 clearly shows that pitting/localized corrosion features are easily distinguishable and their depths can be quantified after cleaning.

Collectively, from the images analyzed for each test specimen, the top 10 deepest features were recorded and averaged to determine an average pit depth. In turn, the mass loss data extracted from each test condition was used to determine an average cumulative thickness loss from the entire steel surface over the 20h period. This calculation is based on the assumption that the mass loss attributed to localized corrosion is substantially smaller than that associated with the material loss generally from the steel surface. Figure 11 helps to support such an analysis as it shows that the number and size of the pits relative to the surrounding area is small, with this image reflecting the behavior observed in other TLC experiments conducted in this study. Finally, the summation of the average pit depth and cumulative general thickness loss produces a total/absolute pit depth. This value is essentially the average depth of the pitting features relative to the original height of the steel surface. Such a value can be used to determine the overall severity of the test conditions by considering the cumulative effect of general and localized corrosion. The methodology also prevents the severity of pitting corrosion in the system from being underestimated in environments where excessive general corrosion is able to significantly mask the true growth/depth of pits.

Figure 12 shows the three different sets of information (average pit depth, cumulative general thickness loss and absolute pit depth) across four test environments both without (Figure 12(a)) and with (Figure 12(b)) 1000ppm HAc. Primarily it is possible to observe that tests performed without HAc (Figure 12(a)) showed a positive linear trend between pit depth and temperature i.e. as temperature increases, so too does the average pit depth and the absolute pit depth. Despite differences in the WCR values across this system, temperature appears to have the overriding effect on the propagation of pits in the non-corrosion product forming environments evaluated here in the absence of HAc.

The addition of HAc (Figure 12(b)) in general creates a more complex response. Through comparison of the test conditions at 20.5^{o}C, the addition of HAc leads to a reduction in average and absolute pit depth. Such observations are in agreement with the suppression (or lack of accentuation) of general corrosion in this test environment. This response is interesting as HAc is normally associated with accentuating localized/pitting corrosion, yet under these specific conditions it is shown to reduce both pit depth and, arguably also general corrosion over 20h. Comparing the remaining three test conditions in Figure 12(b), the addition of HAc leads to an increase in average and absolute pit depth compared to the same system in the absence of the weak acid. However, one key difference is that the test condition at 42.5^{o}C has a higher absolute pit depth compared to the experiment at 50.3^{o}C. This shows a more complex interrelation between WCR and T_s in terms of localized corrosion when HAc is present in the system.

According to previous TLC experiments[14,34] at low temperatures localized corrosion issues are rarely observed in wet-gas multiphase flow conditions, aligning with the observation here of very shallow pitting features which are similar to the general thickness loss rate. It is also important to state that even though no corrosion product layer was formed during these short term tests, initiation of localized corrosion was observed after 20h of test. This pit initiation may be associated with the preferential ferrite consumption that is increased due to the development large cathodic areas of Fe_3C. This phenomena results in a galvanic coupling effect that, along with local chemistry changes, initiates and increases the depth of pits, as suggested in previous studies.[15,17] The localized ferrite consumption is intensified by the addition of HAc, as recorded by the

rougher profiles consisting of several peaks and valleys. As already mentioned, such increased preferential dissolution will increase the ratio of Fe_3C to ferrite over time. Pessu *et al.*[35] presented a study correlating the evolution of different forms of corrosion products at different bulk pH and pitting corrosion in active materials in CO_2 environments. Tests performed on X65 steel at pH 3.8 (unbuffered) showed pitting corrosion (relative to corroded surface) occurred steadily, with pit depths around 10µm developing after 7h of test, even though Fe_3C was the only species observed on the steel surface after the tests. The authors also pointed out that the high general corrosion rate observed at acid medias (pH <4) has the ability to essentially mask the depth of initiated pits which was related to metal penetration occurring at a faster rate than that recorded from purely profilometry depth analysis.[35,36]

3.5.2 Long term localized corrosion (96h).

Despite clear indications of pitting after 20h of exposure to TLC conditions, it is not possible to know from a single test period whether the pits identified will continue to propagate. In order to obtain more information regarding the propagation of pits, longer term (96h) experiments were conducted, and subjected to the same method of profilometry analysis. However, only two conditions were selected for the extended duration study; T_s = 50.3°C and T_s = 20.5°C.

Long term tests performed at T_s = 50.3°C without HAc showed that the high temperature and longer time of exposure may favor the precipitation of $FeCO_3$ layer. However, the film precipitation was non-uniform, mainly consisting of sparsely distributed clusters throughout the metallic surface. Previous studies showed that the non-uniformity of $FecO_3$ coverage is a result of water renewal which continuously brings freshly aggressive water that alters the local chemistry.[15] Figure 13 presents a summary of the relationship between average pit depths (relative to corroded surface) and cumulative thickness loss resulting from uniform corrosion as well as the total/absolute pit depth. At both temperatures, pits and localized features continue to propagate. Relatively shallow pits and features (<15 µm) are observed at the lower temperature of 20.5°C, both with and without HAc. Over the longer duration experiment of 96h, the presence of 1000ppm HAc appears to have no significant effect on the propagation of pits, neither accelerating nor decelerating their growth. The inhibitory effects of HAc with regards to general and localized corrosion are less pronounced at longer durations. That being said, there is still no significant accentuation of either degradation process at the lower temperature as a result of the introduction of 1000ppm HAc into the bulk solution, despite increased aggressiveness of the condensate, (lower pH) suggesting some maintained action of HAc as a weak inhibitor.

At the higher temperature of 50.3°C, when considering the absolute pit depth, there is a noticeable acceleration of pit growth upon the introduction of 1000ppm HAc to the system. However, one can observe that much of the absolute pit depth at the higher temperature is a result of the high thickness loss from the general attack. Further analysis on the influence of the initiation of $FeCO_3$ precipitation in such environments and its influence in localization of TLC will be better accessed in future publications,

4 CONCLUSIONS

This paper evaluates the general and localized top-of-line corrosion (TLC) behavior of X65 carbon steel and the role of acetic acid (HAc) across a range of surface temperatures (T_s from 20.5 to 50.3°C) and water condensation rates (WCRs from 0.07 to 0.81mL/m^2.s) using a newly designed TLC test rig. The rig is able to provide information on T_s, WCRs, real-time *in-situ* corrosion rates (using miniature electrodes) and integrated corrosion rates (using mass loss specimens). The work presented is complemented by surface analysis techniques to confirm the presence of ferrous acetate on the steel surface when HAc is introduced to the bulk solution. In addition, 3D profilometry is implemented to enable pit growth and susceptibility to be investigated. The main conclusions from this study are:

- The developed miniature electrodes are able to provide valuable information on the time-dependent corrosion rate of carbon steel in a TLC environment. Furthermore, comparison of the integrated corrosion rates from the electrochemical response with mass loss measurements highlights the validity of the approach.

- Depending upon the environments studied, the introduction of 1000ppm HAc to the bulk solution in a CO_2-TLC environment was shown to either accentuate, slightly inhibit or have no significant effect on general and localized steel dissolution.

- At near room temperature HAc has no significant effect on, or acted as a weak inhibitor of steel dissolution where the acidification of the environment did not result in the increase of both general and localized corrosion as observed in all other tested conditions. The ability of HAc to suppress the corrosion rate was attributed the formation of ferrous acetate, which was characterized and verified by a combination of FTIR and XPS analysis. These findings are in accordance with assumptions reported in other studies in bulk fluid environments.

- In the three other higher surface temperature environments evaluated, an increase in general and localized corrosion rate was observed due to the presence of 1000ppm HAc in the bulk solution. The extent of corrosion rate accentuation in each environment indicated the complex nature of the system when HAc is present. It was clear that the effects which accentuate corrosion (reduced condensate pH, buffering effect provided by HAc and synergy between HAc and temperature) and those which can cause a reduction in corrosion rate (increase of pH in droplet due to dissolution and inhibition effect caused by HAc) were actively competing against one another.

- Localized corrosion initiation was observed in short term tests (20h) without the presence of HAc, having a direct relation with the surface temperature. With the exception of the lower surface temperature test (20.5°C) the addition of 1000ppm HAc resulted in more aggressive general corrosion behavior which masked the true growth and extent of pitting. This warranted consideration of the absolute pit depth as a measure of localized corrosion susceptibility and indicated that pitting was accentuated in all tests with the exception of the lowest temperature environment (20.5°C)

- At the lower temperature of 20.5°C, longer duration experiments (96h) showed less pronounced inhibitory effects of HAc towards general and pitting corrosion. At the higher surface temperature of 50.5°C, pitting and general corrosion continued undisrupted and were accentuated by 1000ppm HAc addition to the bulk solution.

5 ACKNOWLEDGMENTS

The authors would like to thank the financial support of CNPq (Brazilian National Council for Scientific and Technological Development) and Shell Brazil on this project. . We would also like to acknowledge the support from the Henry Royce Institute (EPSRC grants: EP/P022464/1, EP/R00661X/1), which funded the VXSF Facilities, within the Bragg Centre for Materials Research at Leeds, and the EPSRC National Facility for XPS ("HarwellXPS"), operated by Cardiff University and UCL, under Contract No. PR16195 who performed the XPS data collection for the presented in this paper.

6 REFERENCES

1. T. Tran, B. Brown, S. Nešić, B. Tribollet, "Investigation of the Mechanism for Acetic Acid Corrosion of Mild Steel". CORROSION 2013, paper no. 2487 (Orlando, FL: NACE, 2013).

2. J. Amri, et al. "Propagation and arrest of localized attacks in carbon dioxide corrosion of carbon steel in the presence of acetic acid." Corrosion 66, 3 (2010), p. 035001-035001.
3. M. SINGER, et al. "CO_2 top-of-the-line corrosion in presence of acetic acid: a parametric study." Corrosion 69, 7 (2013), p. 719-735, 2013.).
4. D. Hinkson, M. Singer, Z. Zhang, S. Nešić, "A Study of the Chemical Composition and Corrosivity of the Condensate in Top of the Line Corrosion". CORROSION 2008, paper no. 08466 (New Orleans, LA: NACE 2008).
5. A. Kahyarian, et al., "Acidic corrosion of mild steel in the presence of acetic acid: Mechanism and prediction," *Electrochimica Acta,* 258(2017), p. 639-652.
6. M. Singer, S. Nesic, Y. Gunaltun. "Top of the line corrosion in presence of acetic acid and carbon dioxide." CORROSION 2004, paper no. 04377 (New Orleans, LA: NACE, 2004).
7. Kahyarian, et at. "Electrochemistry of CO_2 corrosion of mild steel: Effect of CO_2 on iron dissolution reaction." *Corrosion Science* 129 (2017), p. 146-151.
8. E. Gulbrandsen, K. Bilkova, "Solution chemistry effects on corrosion of carbon steels in presence of CO2 and acetic acid." CORROSION 2006, paper no. 6364 (San Diego, CA: NACE 2006).
9. J.L. Crolet, N. Thevenot, A. Dugstad, "Role of free acetic acid on the CO_2 corrosion of steels." CORROSION 99, paper no. 24 (San Antonio, TX: NACE 1999).
10. S.S. De Carvalho, et al., "Development and evaluation of miniature electrodes for electrochemical measurements in a CO_2 top-of-line corrosion environment". Corrosion Engineering, Science and Technology, p. 1-9, 2019.
11. ASTM G102-89. (1999). Standard practice for calculation of corrosion rates and related information from electrochemical measurements.
12. ASTM G46-94. (2005). Standard guide for examination and evaluation of pitting corrosion.
13. D. Larrey, Y.M. Gunaltun, "Correlation of cases of top-of-line corrosion with calculated water condensation rates. CORROSION 2000, paper no. 00071 (Orlando, FL: NACE 2000).
14. M. Singer, *16-Top-of-the-line corrosion in Trends in Oil and Gas Corrosion Research and Technologies*, Woodhead Publishing (2017), p. 385-408.
15. J. R. Shant, R. Barker, A. Neville. "Variation of Top-of-line Corrosion Rates at Different Positions in Pipe." India Oil and Gas Pipeline Conference, paper no. 2438 (Mumbai, India: ASME 2017).
16. P. C. Okafor and S. Nesic. "Effect of acetic acid on CO_2 corrosion of carbon steel in vapor-water two-phase horizontal flow." *Chemical Engineering Communications,* 194, 2 (2007), p. 141-157.
17. M. M. Islam et al., "Study of the top-of-the-line corrosion using a novel electrochemical probe". *Corrosion*, *74*, 5 (2017), p. 588-598.
18. Y.S. Choi, S. Nešić. "Determining the corrosive potential of CO_2 transport pipeline in high pCO_2 – water environments," *International Journal of Greenhouse Gas Contro*l 5, 4 (2011), p. 788-797.
19. M.B. Kermani et al., "Carbon dioxide corrosion in oil and gas production - a compendium." *Corrosion 59*, 8(2003), p. 659-683.
20. Chembook CAS: 3094-87-9, https://www.chemicalbook.com/SpectrumEN_3094-87-9_IR1.htm (last accessed 05/mar/2020)
21. A.Q. Wang and T.D. Golden. "Electrodeposition of oriented cerium oxide films," *International Journal of Electrochemistry*, (2013).
22. L.H. Jones, and E. McLaren, "Infrared spectra of CH_3COONa and CD_3COONa and assignments of vibrational frequencies," *Journal of Chemical Physics*, 22, 11, (1954), p. 1796–1800.
23. J.K. Kim, et al. "Recovery of iron as a form of ferrous acetate precipitates from low-grade magnetite ore." *Chemical Engineering Research and Design*, 88, 11 (2010), p. 1467-1473.
24. S., Dorey, F., Gaston, S.R. Marque, B. Bortolotti, and N. Dupuy, "XPS analysis of PE and EVA samples irradiated at different γ-doses." *Applied Surface Science*, *427* (2018), p.966-972.
25. I. Samusawa and S. Kazuhiko, "Influence and role of ethanol minor constituents of fuel grade ethanol on corrosion behavior of carbon steel." *Corrosion Science* 90 (2015), p. 266-275.

26. Thermo scientific XPS simplified, https://xpssimplified.com/periodictable.php (last accessed 05/mar/2020)
27. S. Sinha, and M. Mukherjee. "A study of adventitious contamination layers on technically important substrates by photoemission and NEXAFS spectroscopies." *Vacuum,* 148 (2018), p. 48-53.
28. G. Greczynski and L. Hultman. "C1s peak of adventitious carbon aligns to the vacuum level: dire consequences for material's bonding assignment by photoelectron spectroscopy." *ChemPhysChem,* 18, 12 (2017), p. 1507-1512.
29. K. Idczak, R. Idczak and R. Konieczny, "An investigation of the corrosion of polycrystalline iron by XPS, TMS and CEMS." *Physica B: Condensed Matter*, 491 (2016), p.37-45.
30. F. Bonnet, F. Ropital, P. Lecour, D. Espinat, Y. Huiban, L. Gengembre, Y. Berthier, and P. Marcus. "Study of the oxide/carbide transition on iron surfaces during catalytic coke formation." *Surface and Interface Analysis: An International Journal devoted to the development and application of techniques for the analysis of surfaces, interfaces and thin films,* 34, 1 (2002), p. 418-422.
31. J.K. Heuer, and J.F. Stubbins, "Microstructure analysis of coupons exposed to carbon dioxide corrosion in multiphase flow." Corrosion, 54, 7(1998), p.566-575.
32. J.K. Heuer, and J.F. Stubbins, "An XPS characterization of $FeCO_3$ films from CO_2 corrosion." *Corrosion Science*, 41, 7(1999), p.1231-1243.
33. A.P. Grosvenor, B.A. Kobe, M.C. Biesinger, and N.S. McIntyre, "Investigation of multiplet splitting of Fe 2p XPS spectra and bonding in iron compounds." *Surface and Interface Analysis: An International Journal devoted to the development and application of techniques for the analysis of surfaces, interfaces and thin films, 36, 12(2004), p.1564-1574.*
34. Y-H Sun, T. Hong, and W. P. Jepson, "Corrosion under Wet Gas Conditions," Corrosion 01, paper no.01034, (Houston, TX: NACE International, 2001).
35. F. Pessu, R. Barker, and A. Neville, "The influence of pH on localized corrosion behavior of X65 carbon steel in CO_2-saturated brines." *Corrosion*, 71, 12 (2015), p. 1452-1466.
36. F. Pessu, R. Barker, and A. Neville. "Pitting and uniform corrosion of X65 carbon steel in sour corrosion environments: the influence of CO_2, H_2S, and temperature." *Corrosion* 73,9 (2017), p. 1168-1183.

7 FIGURE CAPTIONS

FIGURE 1. a) Mass loss specimens and b) the developed miniature electrodes consisting of two Hastelloy® c276 wires as reference and counter electrodes and a X65 steel wire, isolated and flush mounted inside a larger X65 specimen.

FIGURE 2. Top-of-line corrosion setup: a) schematic diagram of the entire TLC experimental setup; b) glass cell and customised lid with cooling matrix.

FIGURE 3. Top-of-line corrosion rates over 20 h for API 5L X65 steel exposed to the vapor produced from a CO_2-saturated 3.5 wt.% NaCl brine with 0 and 1000 ppm of HAc and respective percentage of computed data at a) WCR = 0.81 mL/m^2.s and T_s = 42.5^{o}C, b) WCR = 0.5 mL/m^2.s and T_s = 50.3^{o}C, c) WCR = 0.2 mL/m^2.s and T_s = 20.5^{o}C, d) WCR = 0.07 mL/m^2.s and T_s = 32.5^{o}C, and, e) Ratio of of non-recorded data points due to loss of connectivity during 20 h of TLC tests in the four different surface temperatures with 0 and 1000ppm HAc.

FIGURE 4. (a) Comparison between mass loss and averaged corrosion rates from electrochemical measurements in this work to demonstrate the accuracy and validity of the miniature electrode configuration (tests are with and without 1000 ppm HAc), and (b) comparison of mass loss and electrochemical corrosion rates acquired in this present work with those reported under comparable conditions in the literature in the absence of HAc.

FIGURE5. Tafel polarization curves after 20 h for API 5L X65 steel exposed to the vapor produced from a CO_2-saturated 3.5 wt.% NaCl brine with 0 and 1000 ppm of HAc at a) T_s = 42.5^{o}C and WCR = 0.81 mL/m^2.s, b) T_s = 50.25^{o}C and WCR = 0.5 mL/m^2.s, c) T_s = 20.5^{o}C and WCR = 0.2 mL/m^2.s and d) T_s = 32.5^{o}C and WCR = 0.07 mL/m^2.s; two repetitions of the same experiment are shown for each tested condition.

FIGURE 6. Comparison between average top-of-line corrosion rate after 20 h tests in the different conditions, considering two scenarios regarding what occurs during periods of non-connectivity electrochemical measurement in TLC; either the corrosion rate during non-connectivity is an interpolation between its nearest electrochemical corrosion measurements, or is set to zero.

FIGURE 7. Undissociated HAc concentration in the condensate after 20 h test for the four test environments considered in this study.

FIGURE 8. SEM analysis of the mass loss specimens after 20 h of test in TLC conditions in a CO_2–saturated 3.5 wt.% NaCl environment at at different WCRs and T_s in a) 0ppm HAc, and b) 1000 ppm HAc.

FIGURE 9. FTIR spectra after 20 h of static TLC test at T_s 20.5^{o}C with 0ppm and 1000 ppm acetic acid. Dotted line represents ferrous acetate standard FTIR spectrum.

FIGURE 10. X-ray photoelectron spectra of ferrous acetate standard (99%) and samples after 20 hours of static TLC test at Ts 20.5^{o}C with and without 1000ppm acetic acid, (a) C1s region, (b) O1s and (c) Fe2p region.

FIGURE 11. Example profilometry analysis for TLC specimens in the presence of 0 ppm HAc at WCR = 0.5 mL/m^2.s and T_s = 50.25^{o}C.

FIGURE 12. Summary of relationship between average pit depths (relative to corroded surface) cumulative thickness loss resulting from uniform corrosion (determined via mass loss measurements), and total/absolute pit depth (the summation of the average pit depth and cumulative thickness loss) after 20 h, plotted as a function of the surface temperature, Ts for four systems (a) without and (b) with 1000 ppm HAc.

FIGURE 13. Summary of relationship between average pit depths (relative to corroded surface) cumulative thickness loss resulting from uniform corrosion (determined via mass loss measurements), and total/absolute pit depth (the summation of the average pit depth and cumulative thickness loss) after 96 h, plotted as a function of the surface temperature, Ts for two systems (a) without and (b) with 1000 ppm HAc.

8 TABLES

Table 1: Chemical Composition of API 5L X65 steel

Elements	C	Si	Mn	P	S	Cr	Ni
wt.%	0.18	0.17	0.64	0.015	0.013	0.04	0.03
Elements	Mo	Al	Cu	Co	Ti	V	Fe
wt.%	<0.002	0.017	0.013	0.018	0.002	<0.001	Balance

Table 2: Top-of-line corrosion tests matrix evaluated in this study

Bottom of the line solution	Temperatures				WCR (ml/m².s)	Test Duration (h)
	T_{bulk} (ºC)	T_{gas} (ºC)	T_{ext} (ºC)	T_s (ºC)		
3.5% NaCl; 3.5% NaCl + 1000ppm HAc;	80	70	-10	42.5 ± 1.0	0.81±0.03	20
	80	70	30	50.3 ± 1.0	0.5±0.03	20 and 96
	50	40	-10	20.5 ± 1.0	0.2±0.05	20 and 96
	50	40	30	32.5 ± 0.5	0.07±0.02	20

$T_{ext.}$: Refrigerent temperature controlled by chiller
T_s : Carbon steel surface temperature

Table 3: Summary of the average top-of-line corrosion rate increase with addition of acetic acid.

Ts (ºC)	WCR (ml/m2.s)	Average LPR CR (mm/year)		Average CR change (%)
		0ppm HAc	1000ppm HAc	
20.5	0.2	0.53 ± 0.2	0.43 ± 0.3	-19
32.5	0.07	0.55 ± 0.09	2.22 ± 0.3	303
42.5	0.81	0.84 ± 0.2	2.80 ± 0.4	233
50.3	0.5	1.36 ± 0.4	2.97 ± 0.08	118

Table 4: pH analysis from bulk solution after 20 h of test without and with acetic acid

WCR (ml/m².s)	$T_{surface}$ (°C)	HAc Concentration in bulk	
		Bulk pH_{20h}	Bulk pH_{20h}
		0ppm	1000ppm
0.07	32.5	3.8	3.0
0.2	20.5	4.0	3.1
0.5	50.3	4.2	3.1
0.81	42.5	4.1	3.1

Table 5: Infrared wavenumber (cm^{-1}) assignments found in literature for the free acetate ion of solid sodium acetate, as-prepared ferrous acetate, ferrous acetate (standard and reference) and ferrous acetate corrosion product.

Vibrational mode	Wavenumbers (cm^{-1})				
	Free acetate[22]	Ferrous acetate[20]	Prepared ferrous acetate[21]	Ferrous acetate reference[23]	Ferrous acetate (this work)
CH stretching	2935	2924, 2964	-	2946	2930, 2964
CH_3 deformation	1335, 1347	1360, 1378	1349	1353	1379
OCO stretching	1424	1455	1417, 1450	1419,1446	1465
C-C stretching	929	1032, 1038	931, 943	945, 956	953,1073
OCO deformation	658	618, 661	666	663	652, 710

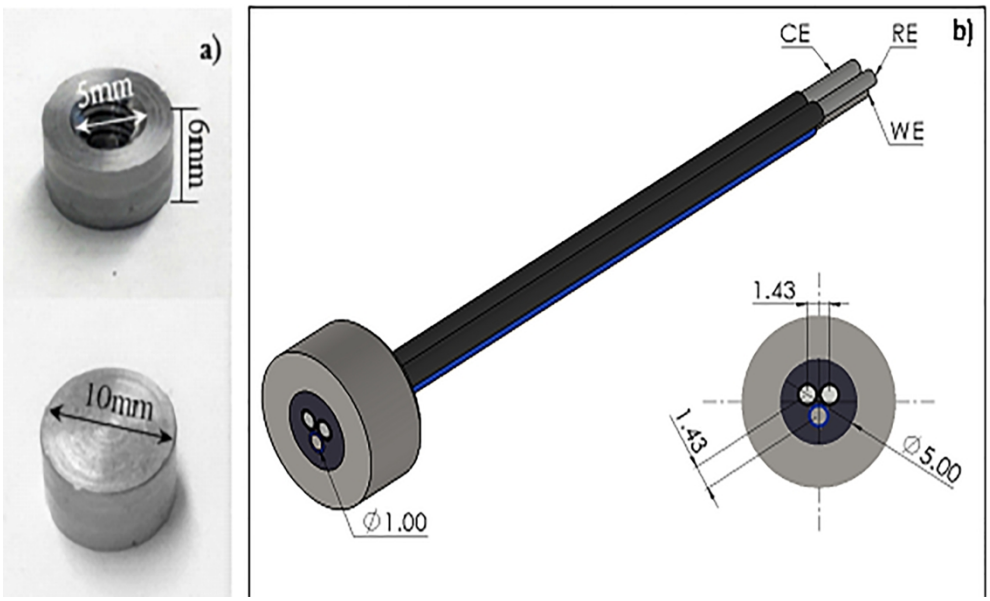

Figure 1. a) Mass loss specimens and b) the developed miniature electrodes consisting of two Hastelloy® c276 wires as reference and counter electrodes and a X65 steel wire, isolated and flush mounted inside a larger X65 specimen.

166x98mm (300 x 300 DPI)

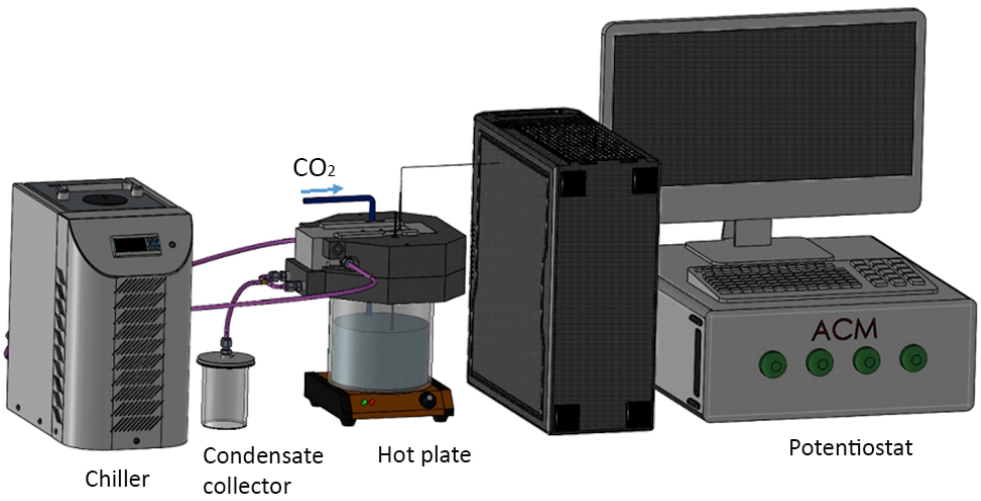

83x44mm (300 x 300 DPI)

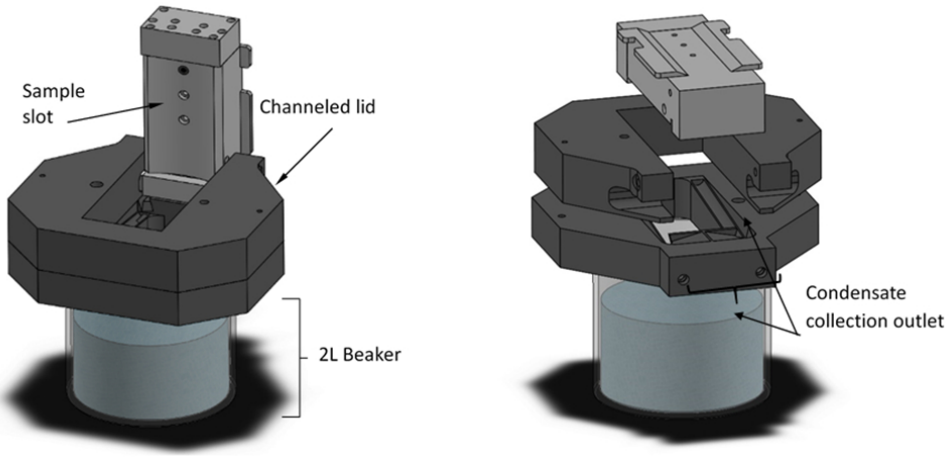

Figure 2. Top-of-line corrosion setup: a) schematic diagram of the entire TLC experimental setup; b) glass cell and customised lid with cooling matrix.

83x38mm (300 x 300 DPI)

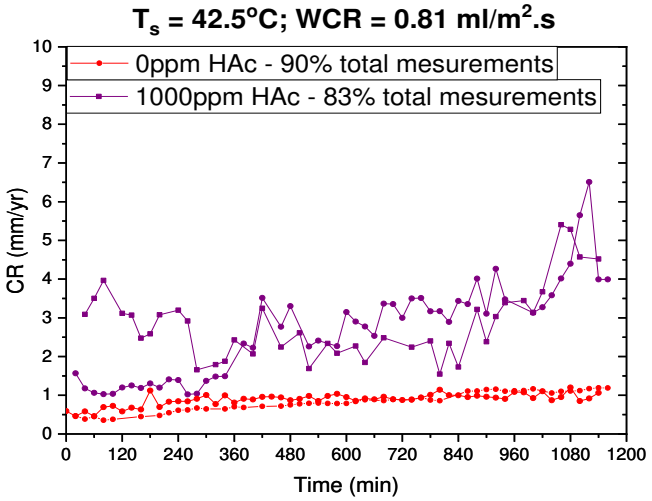

(a)

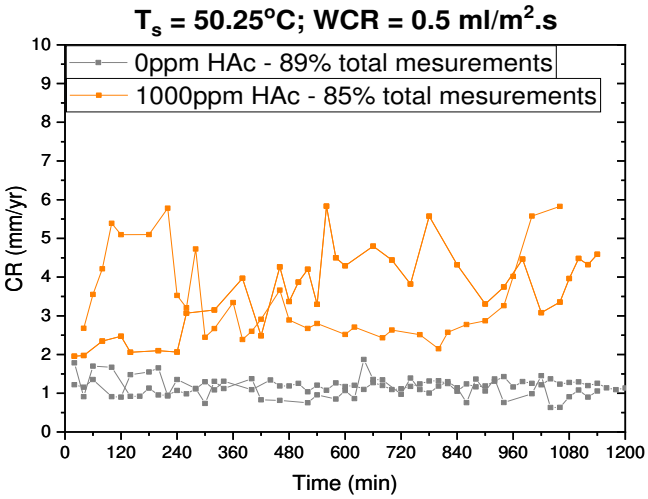

(b)

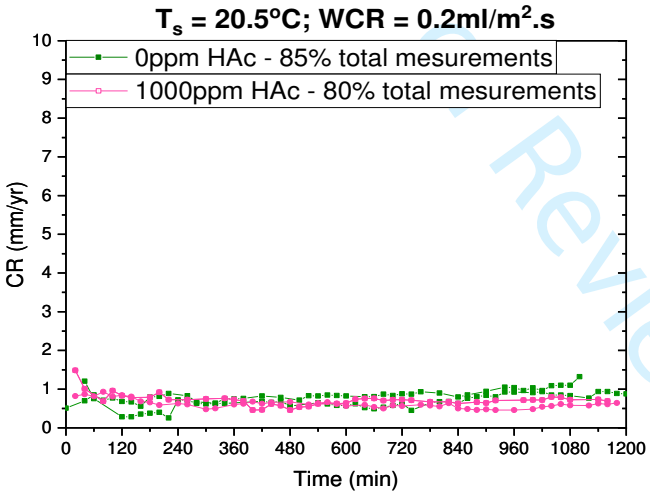

(c)

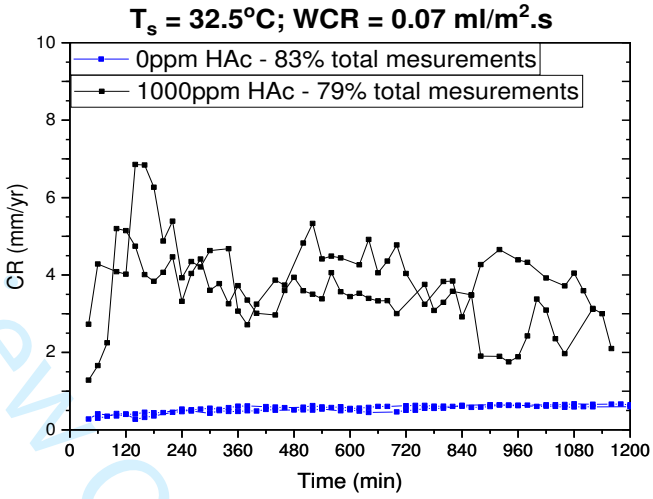

(d)

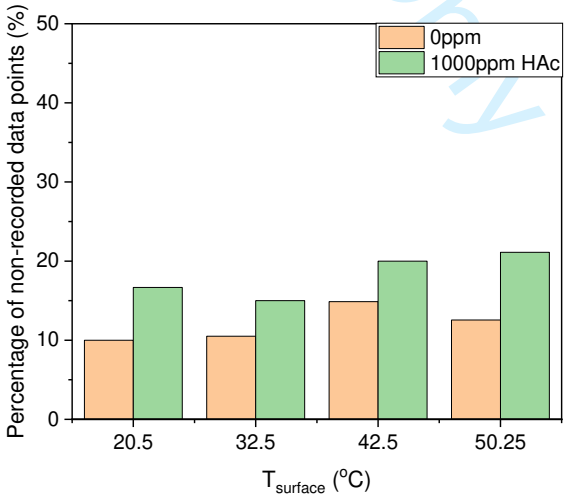

(e)

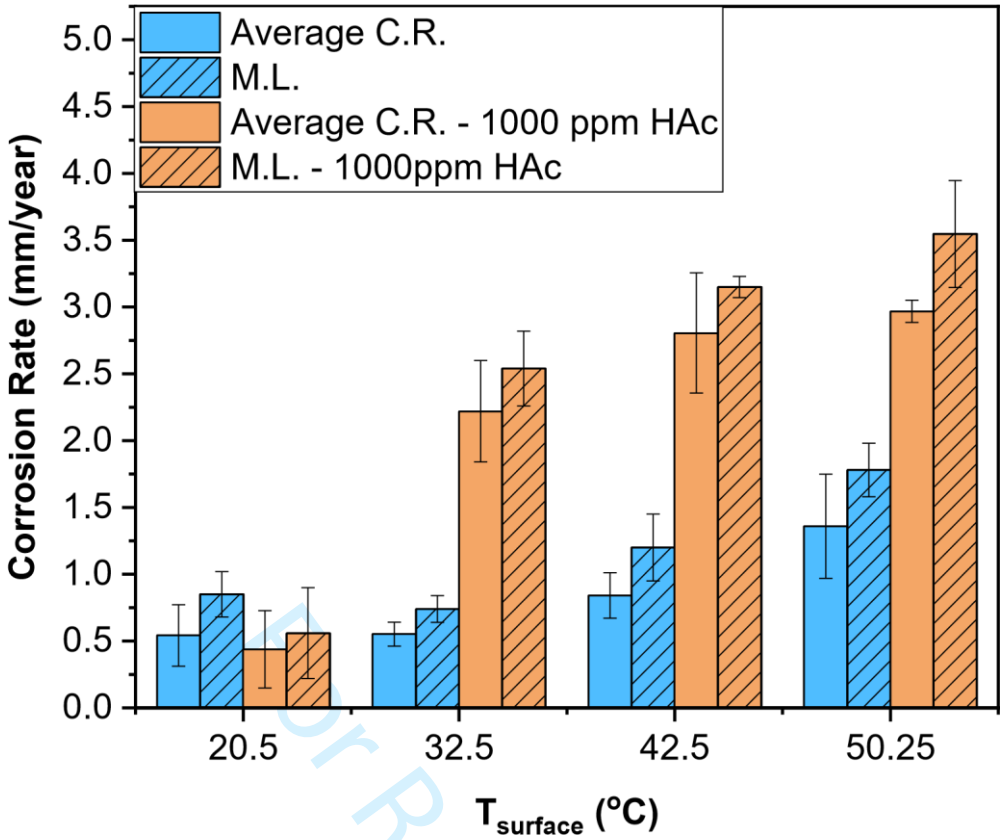

(a)

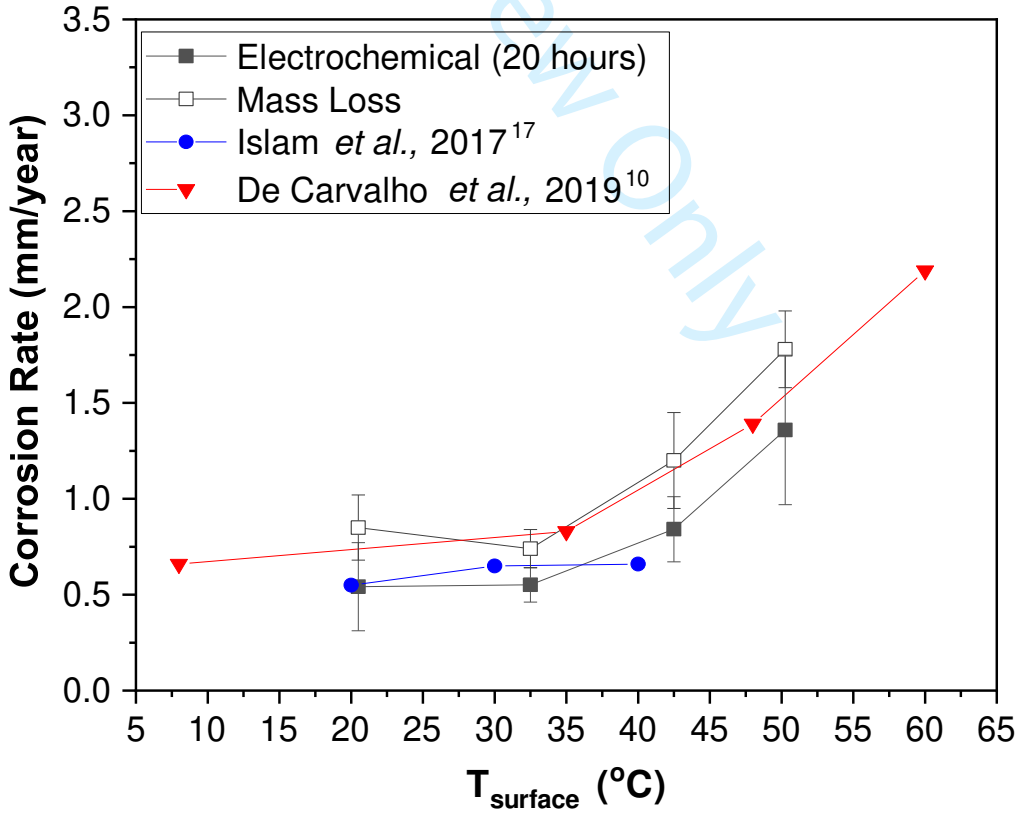

(b)

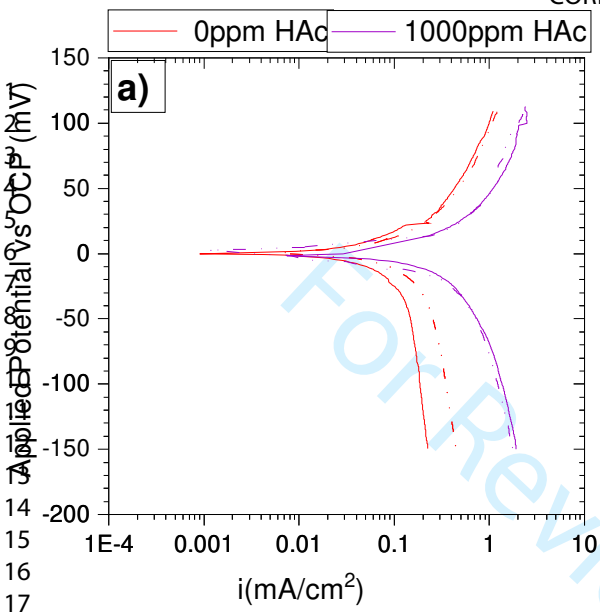

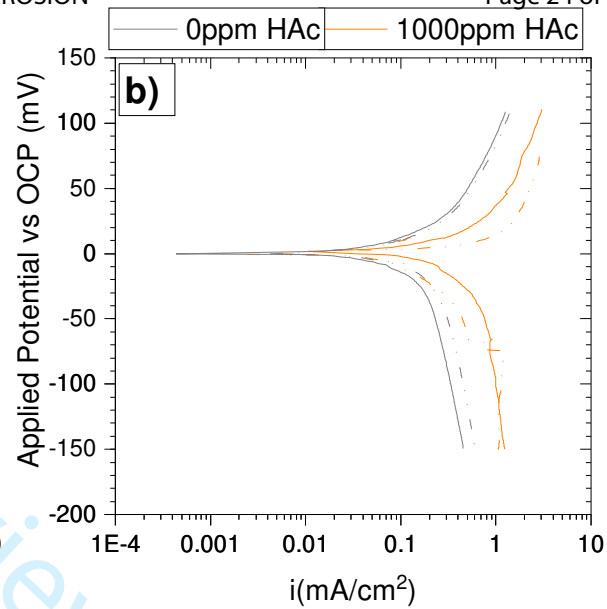

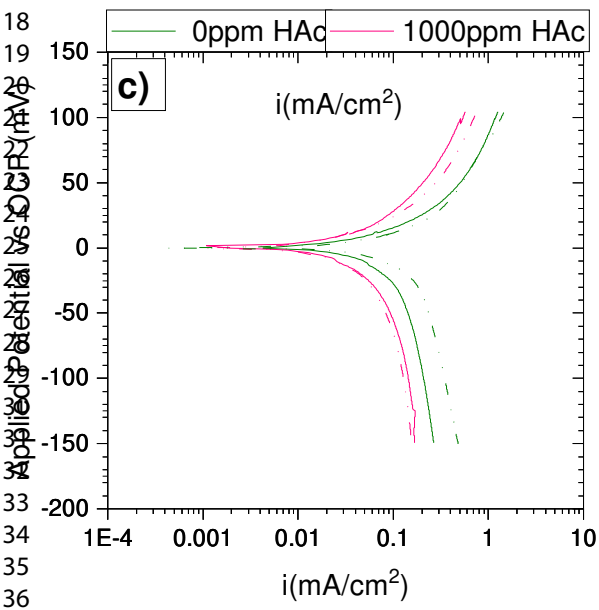

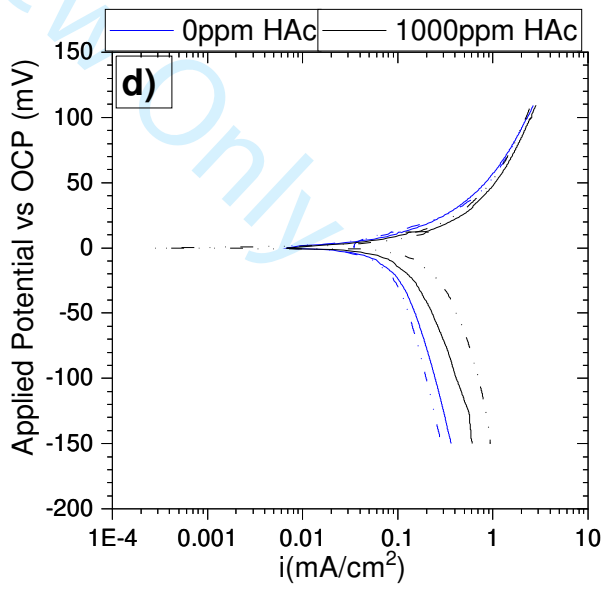

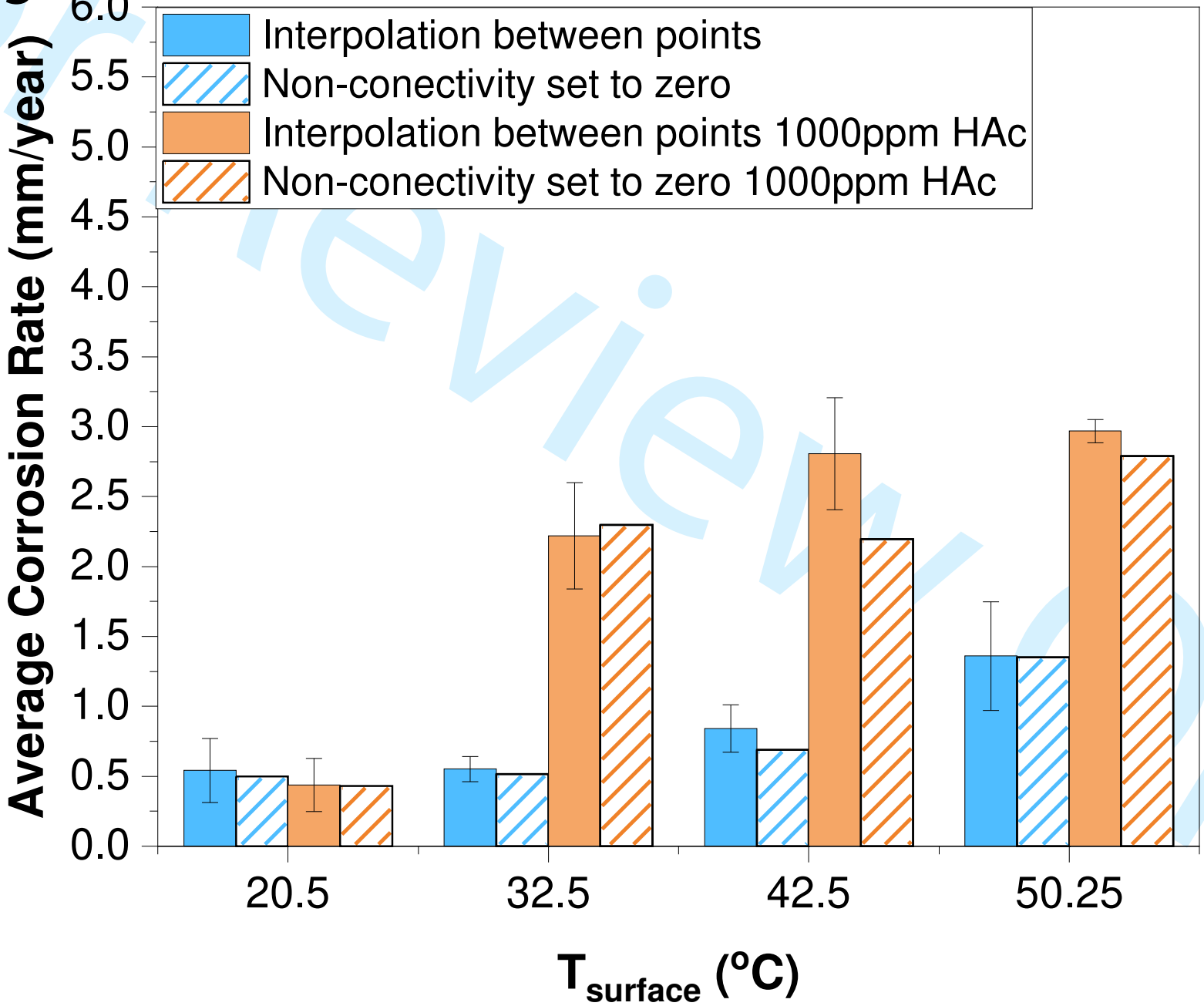

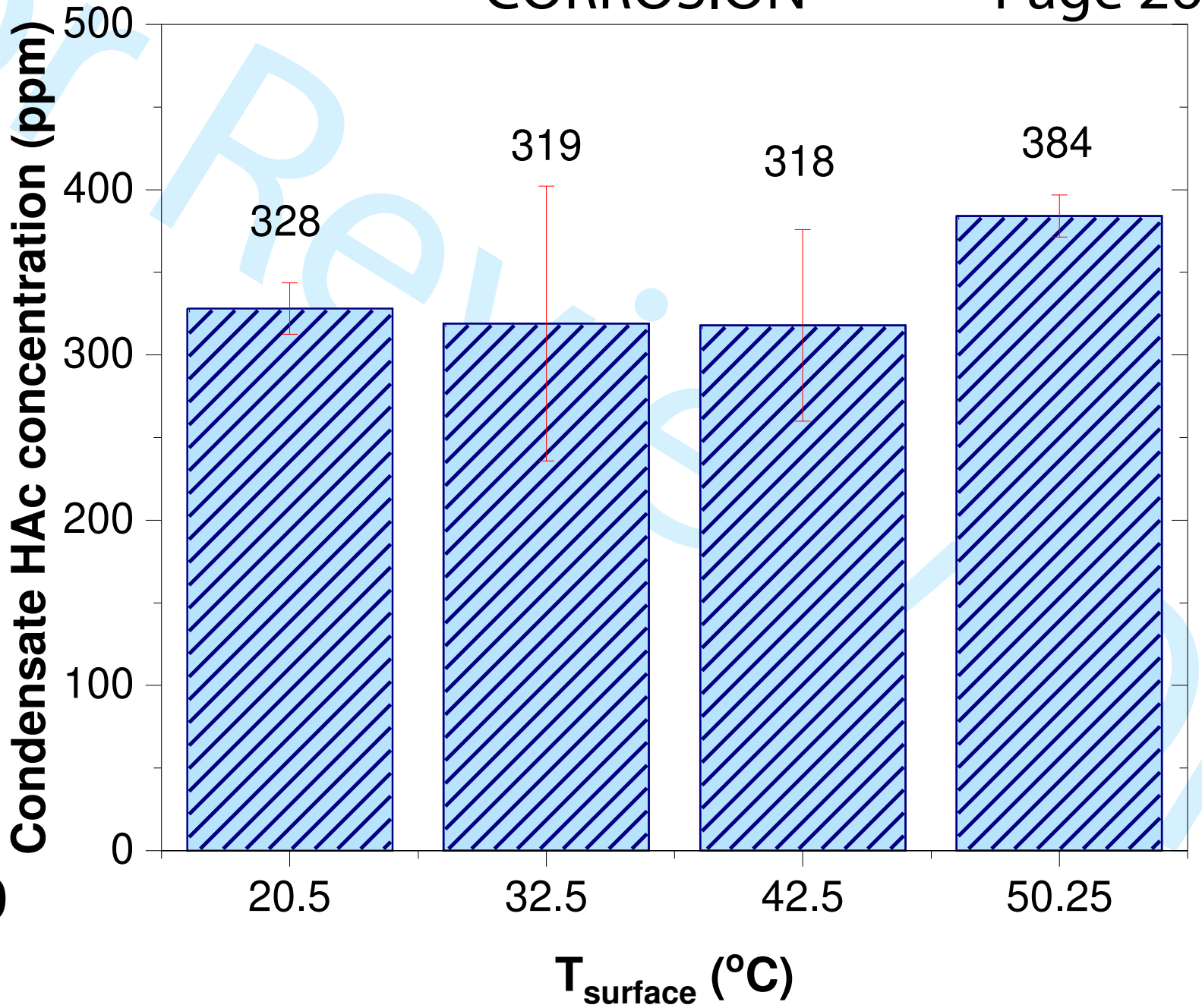

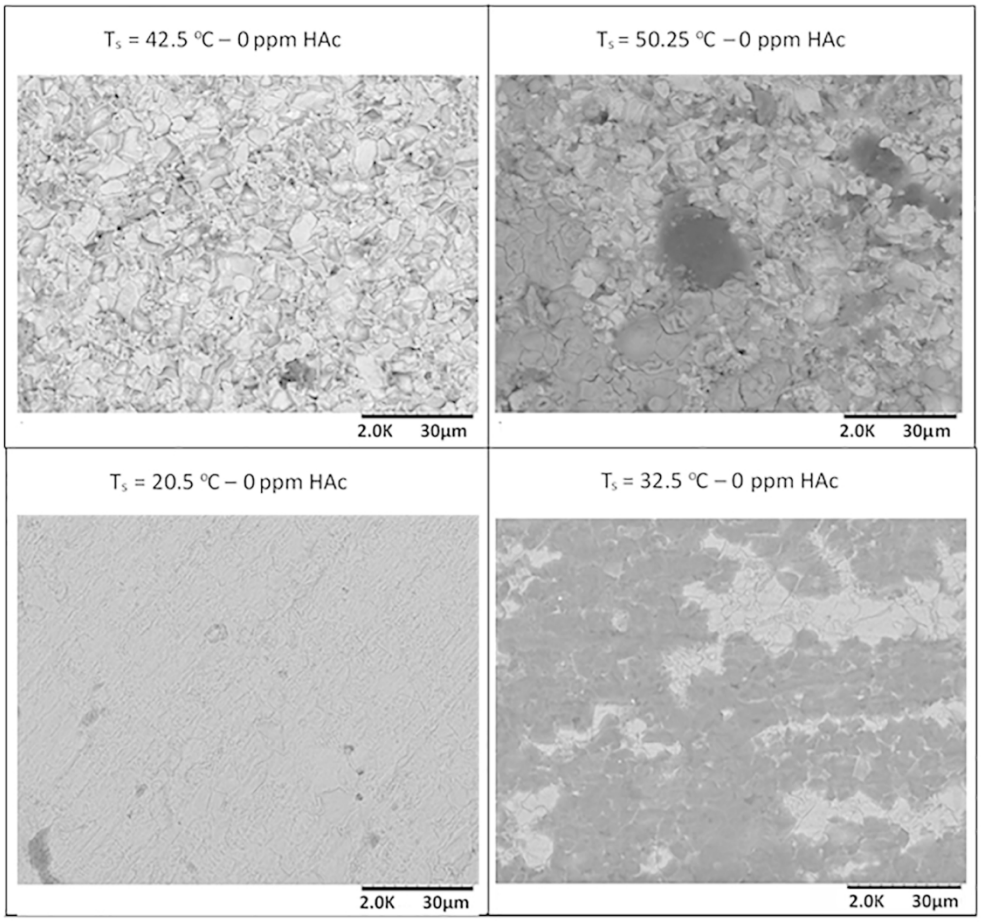

167x154mm (300 x 300 DPI)

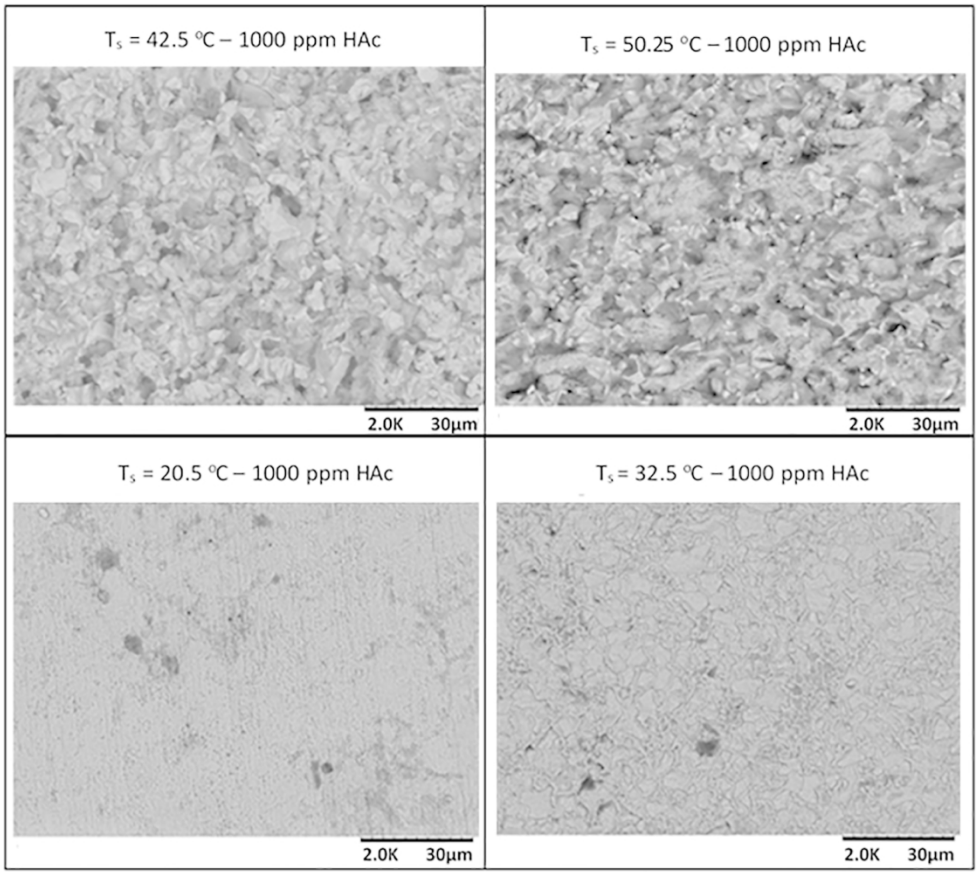

Figure 8. SEM analysis of the mass loss specimens after 20 h of test in TLC conditions in a CO2–saturated 3.5 wt.% NaCl environment at at different WCRs and Ts in a) 0ppm HAc b) 1000ppm HAc

167x154mm (300 x 300 DPI)

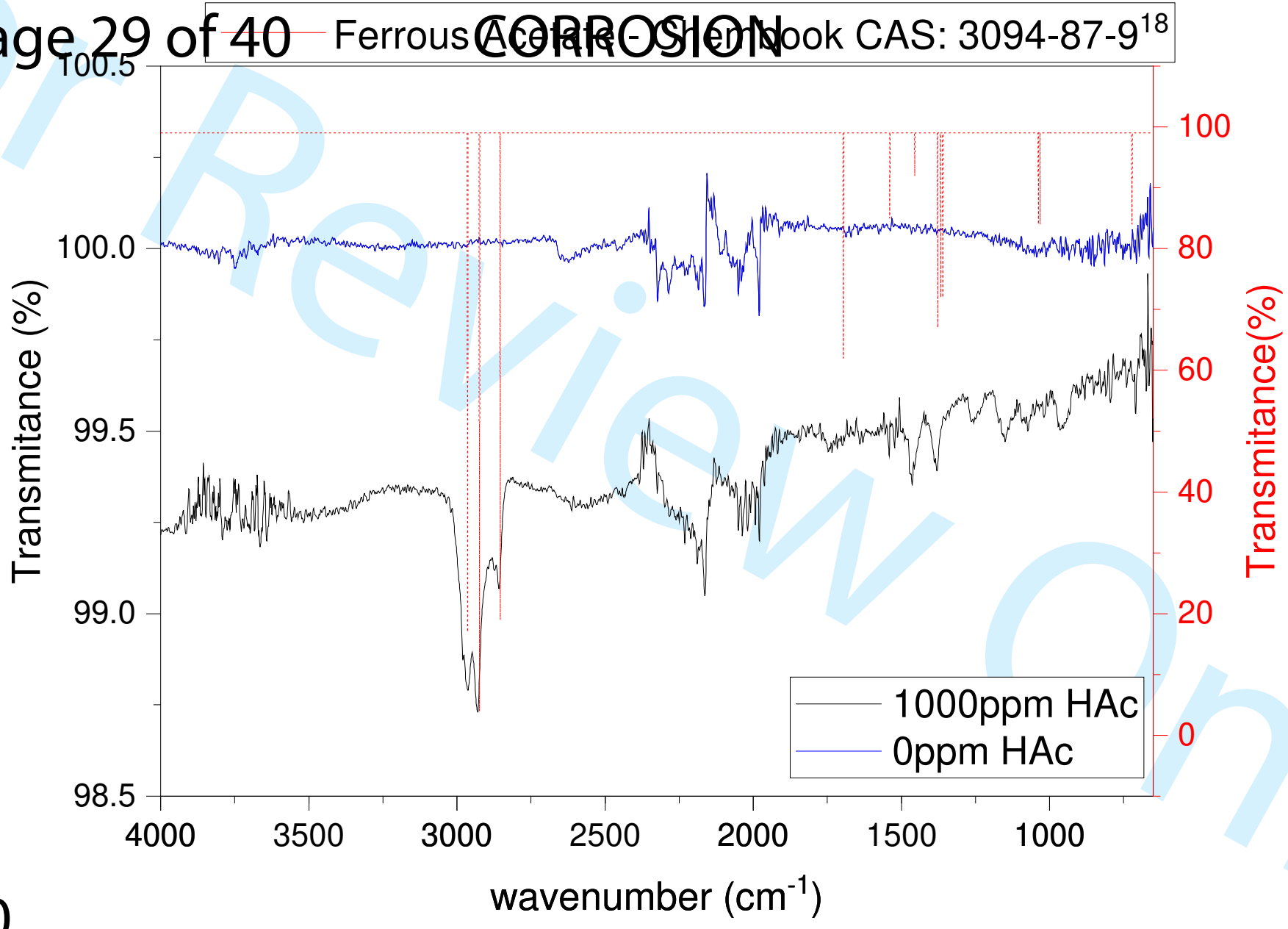

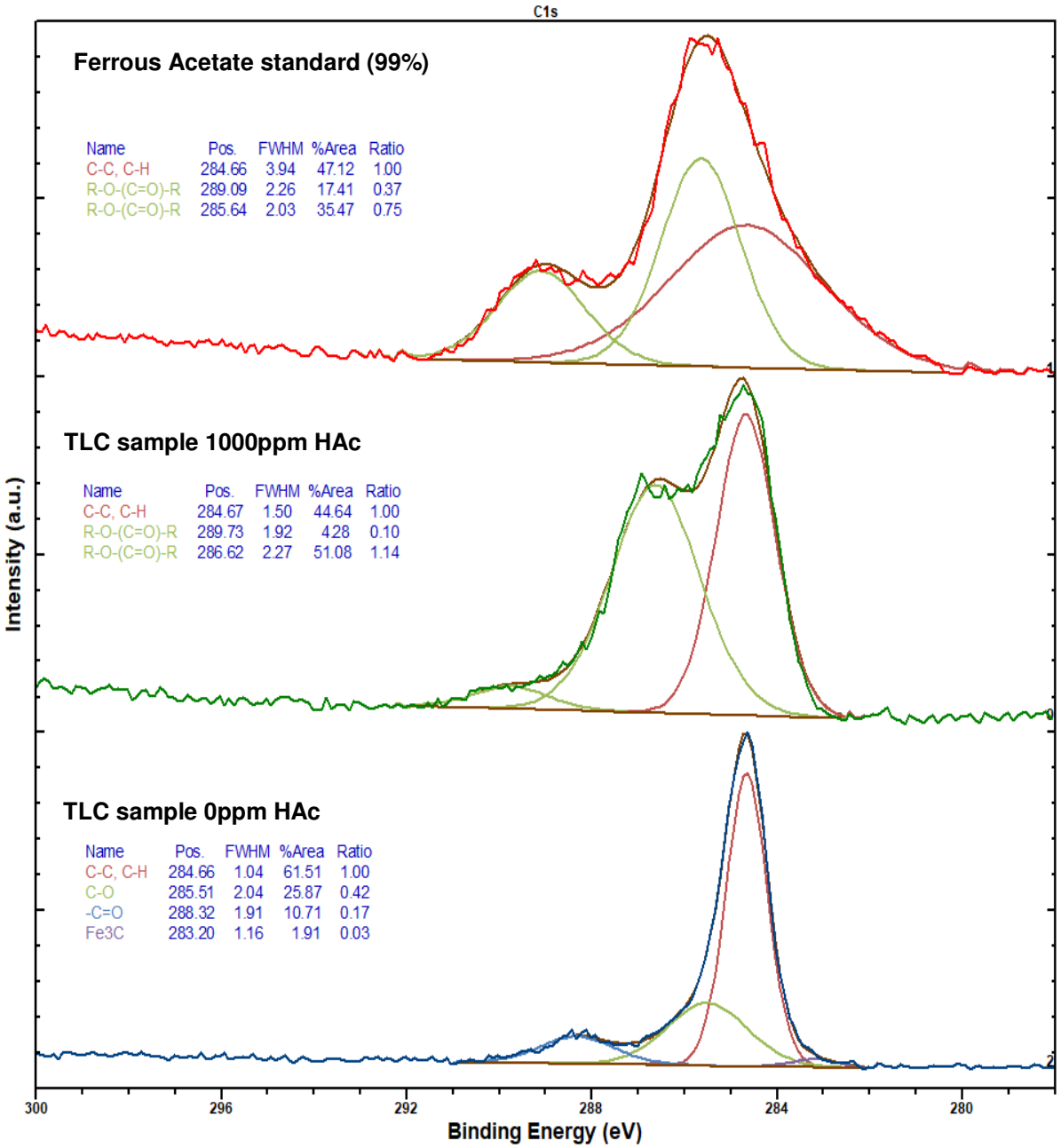
C1s
Ferrous Acetate standard (99%)
Name Pos. FWHM %Area Ratio
C-C, C-H 284.66 3.94 47.12 1.00
R-O-(C=O)-R 289.09 2.26 17.41 0.37
R-O-(C=O)-R 285.64 2.03 35.47 0.75
TLC sample 1000ppm HAc
Name Pos. FWHM %Area Ratio
C-C, C-H 284.67 1.50 44.64 1.00
R-O-(C=O)-R 289.73 1.92 4.28 0.10
R-O-(C=O)-R 286.62 2.27 51.08 1.14
TLC sample 0ppm HAc
Name Pos. FWHM %Area Ratio
C-C, C-H 284.66 1.04 61.51 1.00
C-O 285.51 2.04 25.87 0.42
-C=O 288.32 1.91 10.71 0.17
Fe3C 283.20 1.16 1.91 0.03
Intensity (a.u.)
300
296
292
288
284
280
Binding Energy (eV)

(a)

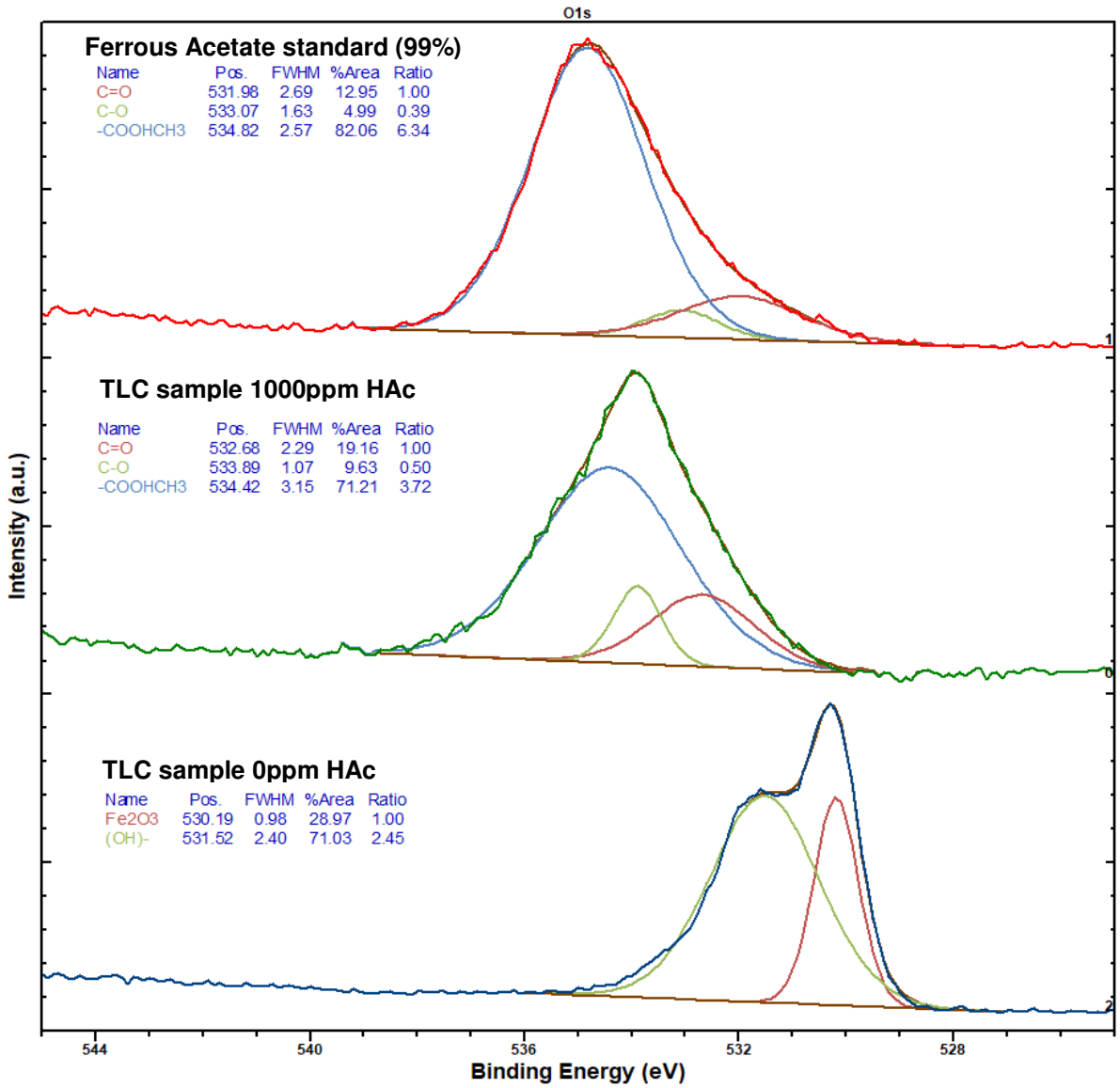
O1s
Ferrous Acetate standard (99%)
Name Pos. FWHM %Area Ratio
C=O 531.98 2.69 12.95 1.00
C-O 533.07 1.63 4.99 0.39
-COOHCH3 534.82 2.57 82.06 6.34
TLC sample 1000ppm HAc
Name Pos. FWHM %Area Ratio
C=O 532.68 2.29 19.16 1.00
C-O 533.89 1.07 9.63 0.50
-COOHCH3 534.42 3.15 71.21 3.72
TLC sample 0ppm HAc
Name Pos. FWHM %Area Ratio
Fe2O3 530.19 0.98 28.97 1.00
(OH)- 531.52 2.40 71.03 2.45
Intensity (a.u.)
544
540
536
532
528
Binding Energy (eV)

(b)

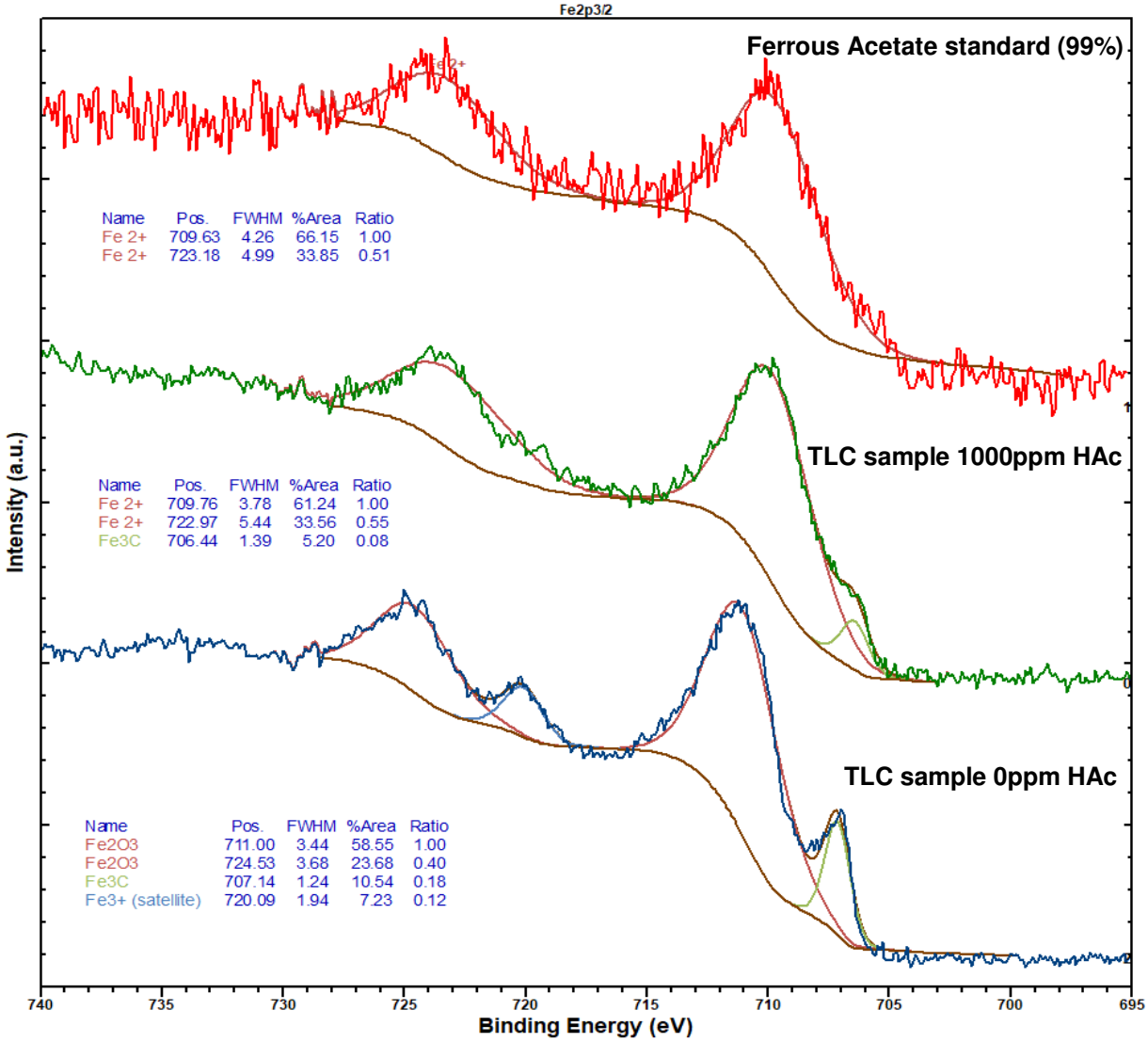
Fe2p3/2
Ferrous Acetate standard (99%)
Fe2+
Name Pos. FWHM %Area Ratio
Fe 2+ 709.63 4.26 66.15 1.00
Fe 2+ 723.18 4.99 33.85 0.51
TLC sample 1000ppm HAc
Name Pos. FWHM %Area Ratio
Fe 2+ 709.76 3.78 61.24 1.00
Fe 2+ 722.97 5.44 33.56 0.55
Fe3C 706.44 1.39 5.20 0.08
TLC sample 0ppm HAc
Name Pos. FWHM %Area Ratio
Fe2O3 711.00 3.44 58.55 1.00
Fe2O3 724.53 3.68 23.68 0.40
Fe3C 707.14 1.24 10.54 0.18
Fe3+ (satellite) 720.09 1.94 7.23 0.12
Intensity (a.u.)
740 735 730 725 720 715 710 705 700 695
Binding Energy (eV)

(c)

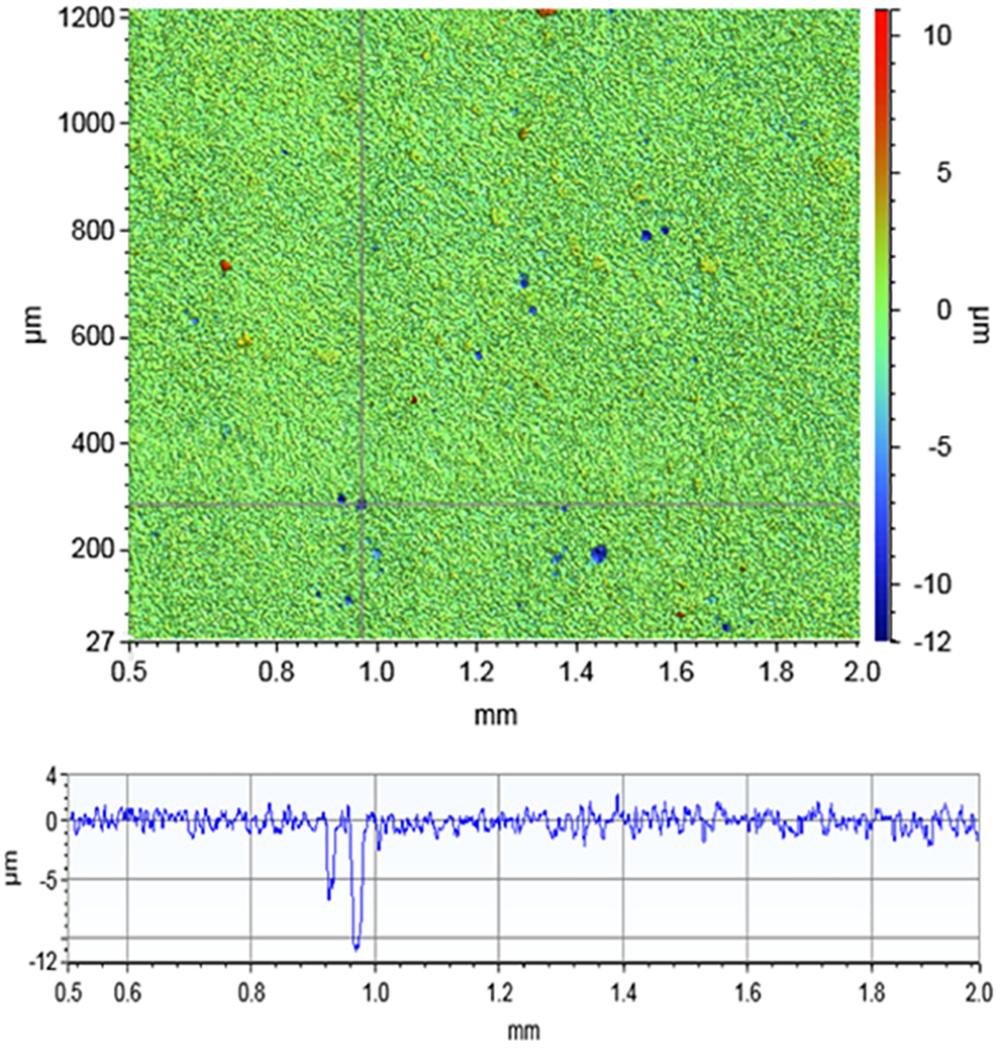

Figure 11. Example profilometry analysis for TLC specimens in the presence of 0 ppm HAc at WCR = 0.5 mL/m2.s and Ts = 50.25oC.

83x89mm (300 x 300 DPI)

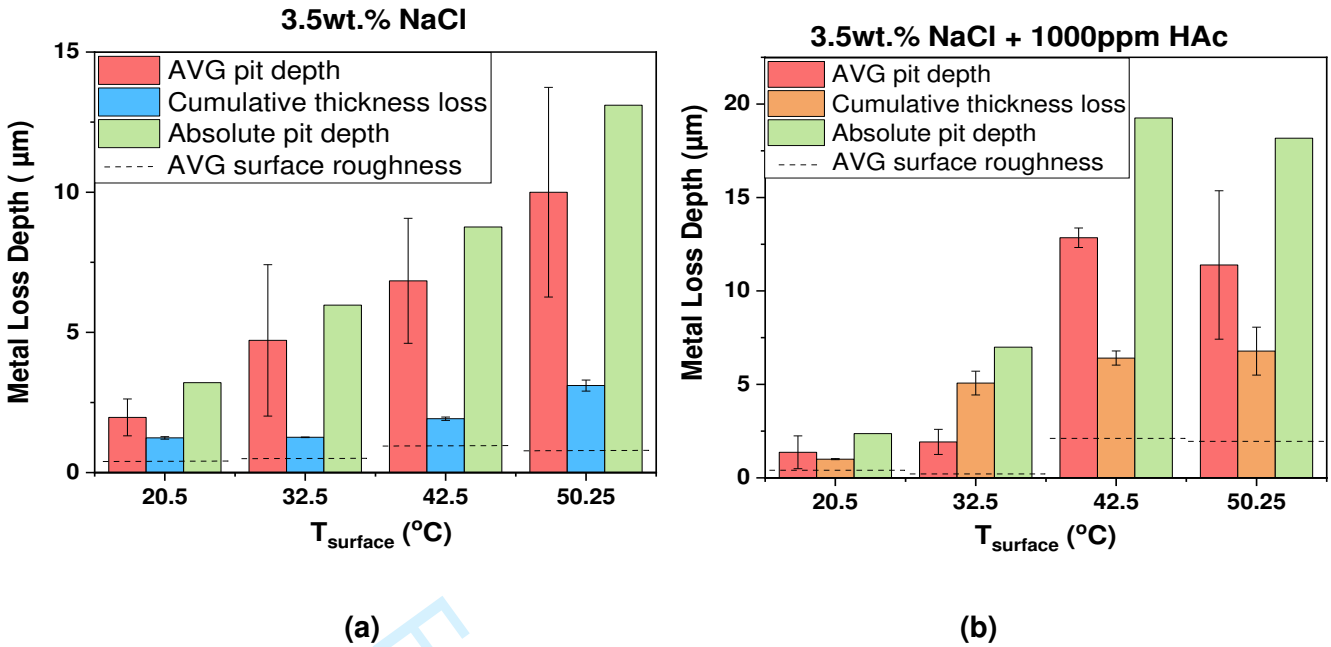

(a) (b)

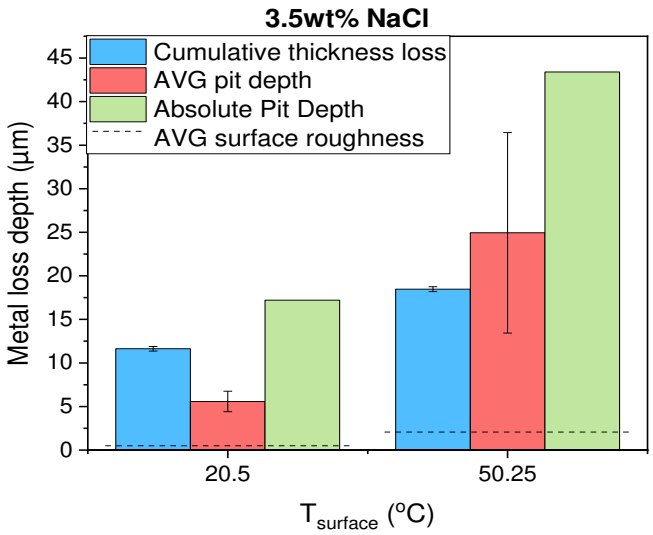

(a)

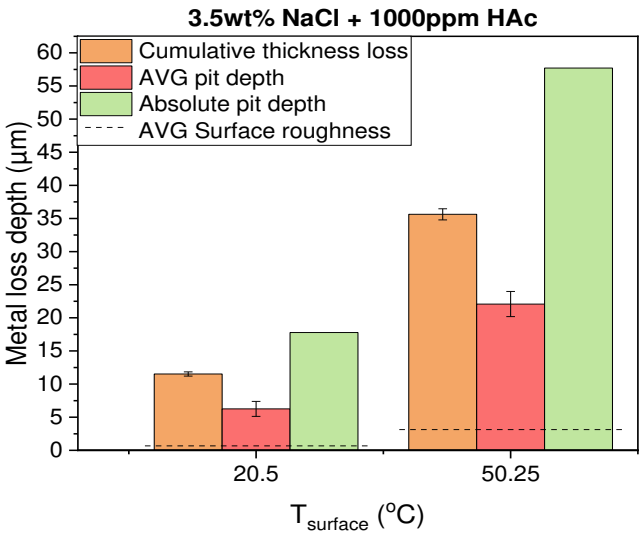

(b)

Table 1: Chemical Composition of API 5L X65 steel

Elements	**C**	**Si**	**Mn**	**P**	**S**	**Cr**	**Ni**
wt.%	0.18	0.17	0.64	0.015	0.013	0.04	0.03
Elements	Mo	Al	Cu	Co	Ti	V	Fe
wt.%	<0.002	0.017	0.013	0.018	0.002	<0.001	Balance

Table 2: Top-of-line corrosion tests matrix evaluated in this study

Bottom of the line solution	Temperatures				WCR (ml/m^2.s)	Test Duration (h)
	T_{bulk} (ºC)	T_{gas} (ºC)	T_{ext} (ºC)	T_s (ºC)		
3.5% NaCl; 3.5% NaCl + 1000ppm HAc;	80	70	-10	42.5 ± 1.0	0.81±0.03	20
	80	70	30	50.3 ± 1.0	0.5±0.03	20 and 96
	50	40	-10	20.5 ± 1.0	0.2±0.05	20 and 96
	50	40	30	32.5 ± 0.5	0.07±0.02	20

$T_{ext.}$: Refrigerent temperature controlled by chiller
T_s : Carbon steel surface temperature

Table 3: Summary of the average top-of-line corrosion rate increase with addition of acetic acid.

Ts (°C)	WCR (ml/m2.s)	Average LPR CR (mm/year)		Average CR change (%)
		0ppm HAc	1000ppm HAc	
20.5	0.2	0.53 ± 0.2	0.43 ± 0.3	-19
32.5	0.07	0.55 ± 0.09	2.22 ± 0.3	303
42.5	0.81	0.84 ± 0.2	2.80 ± 0.4	233
50.3	0.5	1.36 ± 0.4	2.97 ± 0.08	118

Table 4: pH analysis from bulk solution after 20 h of test without and with acetic acid

WCR (ml/m².s)	$T_{surface}$ (°C)	HAc Concentration in bulk	
		Bulk pH_{20h}	Bulk pH_{20h}
		0ppm	1000ppm
0.07	32.5	3.8	3.0
0.2	20.5	4.0	3.1
0.5	50.3	4.2	3.1
0.81	42.5	4.1	3.1

Table 5: Infrared wavenumber (cm^{-1}) assignments found in literature for the free acetate ion of solid sodium acetate, as-prepared ferrous acetate, ferrous acetate (standard and reference) and ferrous acetate corrosion product.

Vibrational mode	Wavenumbers (cm^{-1})				
	Free acetate[20]	**Ferrous acetate[18]**	**Prepared ferrous acetate[21]**	**Ferrous acetate reference[21]**	**Ferrous acetate (this work)**
CH stretching	2935	2924, 2964	-	2946	2930, 2964
CH_3 deformation	1335, 1347	1360, 1378	1349	1353	1379
OCO stretching	1424	1455	1417, 1450	1419,1446	1465
C-C stretching	929	1032, 1038	931, 943	945, 956	953,1073
OCO deformation	658	618, 661	666	663	652, 710